6. QUANTITATIVE ENVIRONMENTAL DESCRIPTION

The Locations Where Data are Provided

6.1.1 Numbering of Sites

The locations were global data are provided are the four deployments sites and 21 transit sites. Typhoon hindcast data is provided at about 2000 points in a grid around the Northwest Pacific deployment site.

Global and deployment sites are referred to within this report by two numbers: the site number, consecutively numbered from 1 – 25, and the Oceanweather grid point number, which being part of a large grid ranges from the 3000s to the 11000s. The correspondence between these numbers is given in Tables 6.1.2-1 and 6.1.3-1.

The typhoon data was created for the region around the Northwest Pacific deployment site, and the Oceanweather grid points are numbered from 5263 to 10425, and no other site numbers were assigned to these locations. These grid points cover a region from latitude 20.125^0 N to 29.8^0 N, and from 125.2437^0 E to 136.9797^0 E. The deployment site (26.0^0N, 131.0^0E) is close to, but not precisely at the middle of this grid. The grid points are spaced at 0.2497^0 east-west and 0.225^0 north-south.

6.1.2 Deployment Sites

Four sites were nominated by the Navy as possible deployment sites. These sites were selected partly as possible locations of future military interest and partly as sites that represent severe environmental conditions.

Site Number	Oceanweather Hindcast Grid Point Number	Lat.	Long.	Description
14	11008	60° N	20° W	North Atlantic Deployment Site
19	8772	22° N	65° E	Arabian Sea Deployment Site
22	9051	26° N	131° E	Western Pacific Deployment Site
23	9796	38° N	131° E	Sea of Japan Deployment Site

Table 6.1.2-1 Location of Deployment Sites

The North Atlantic site (NA) is subjected to severe conditions during a large proportion of the time, with intense storms generating enormous waves. The Northwest Pacific site (NWP) is subjected to periodic intense typhoons that sweep up from the Southeast, but conditions otherwise are more mild. The Sea of Japan (SJ) experiences similar typhoon conditions to NWP, but is sheltered somewhat by the islands of Japan, so that it can be expected to be less severe overall than NWP. Typhoons also move up from the Indian Ocean past the Arabian Sea site (AS), but these are less severe than at NWP. Although monsoons are present at AS with considerable strength and regularity, the winds are not generally as strong as those frequently present at NA.

Figures 6.1.2-1 and 6.1.2-2 show the distribution of significant wave heights at the four sites from a global wave hindcast. These plots suggest that NA (North Atlantic) has the largest waves, but when waves from dedicated typhoon hindcasts of NWP (Northwest Pacific) are considered, equally large waves are found. Thus, either of these two sites could dictate the largest waves for survival conditions. This would govern the strength design in the disconnected state.

The Navy has specified that the critical conditions just before disconnecting are seastate 6 (significant wave height of 5 m). All deployment sites experience seastate 6, so any deployment site could be critical for the disconnecting process, depending on the frequency or directional content of the waves. However, whereas seastate 6 is exceeded only about 1 or 2% of the time at NWP, AS and SJ, it occurs almost 10% of the time at NA.

Figure 6.1.2-2 shows that 50% of the waves at NA are greater than 3-m significant height, while this figure is 23% at NWP and about 15% at the other two sites. From this, it can expected that NA will have the worst conditions for fatigue and operational availability.

Table 6.1.2-2 summarizes the characteristics of each site and suggests which sites may be expected to govern the principal design phases of the MOB. Primary site indicates that this site is expected to govern the design for this condition, but a check should be made for other sites also.

	North Atlantic	West Pacific	Arabian Sea	Sea of Japan	Transit
Percentage of Time	70%	70%	70%	70%	5%
Configuration	Connected, Disconnected, Connecting, Disconnecting	Connected, Disconnected, Connecting, Disconnecting	Connected, Disconnected, Connecting, Disconnecting	Connected, Disconnected, Connecting, Disconnecting	Disconnected, Ballasted, Unballasted
Operations	Aircraft ops., Cargo transfer	Aircraft ops., Cargo transfer	Aircraft ops., Cargo transfer	Aircraft ops., Cargo transfer	Nil
Site Characteristics	Extreme storms; Frequent storms	Extreme typhoons; Milder background	Milder typhoons; Monsoon	Extreme typhoons; Milder background; Sheltered	Extremely varied
Member strength connected (waves)	Primary site	Primary site	Secondary site	Secondary site	Not applicable
Member strength disconnected (waves)	Primary site (ballasted)	Primary site (ballasted)	Secondary site	Secondary site	Primary site (unballasted)
Member strength disconnecting (waves)	Primary site	Primary site	Primary site	Primary site	Not applicable
Fatigue (waves)	Primary site	Secondary site	Secondary site	Secondary site	Primary site (unballasted)

Table 6.1.2-2 Characteristics and Potential Design Requirements of Sites

6.1.2 Transit Sites

After selection of the deployment sites, a number of sites were chosen to represent possible routes of transit. It has not been decided how many MOBs might be built, and where the home port(s) might be. For this reason, it has been assumed that the MOB would traverse all the oceans of the world getting from deployment to deployment, or back to home port, and would even have to pass Cape Horn, since it would be too large to pass through the Panama Canal.

To assess the metocean conditions that could be experienced during transit, likely transit routes were selected as shown in Figure 6.1.3-1. From these, a set of 21 transit sites was selected that covered the principal conditions expected in transit. These are listed in Table 6.1.3-1 and are shown in Figure 6.1.3-2.

Site Number	Oceanweather Hindcast Grid Point Number	Lat.	Long.	Description
1	7797	10° N	170° W	Tropical Central Pacific
2	4794	25° S	140° W	Tropical Central Pacific
3	3343	40° S	140° W	South Eastern Pacific
4	3353	40° S	115° W	South Eastern Pacific
5	8246	15° N	115° W	Tropical Eastern Pacific
6	8248	15° N	110° W	Tropical Eastern Pacific
7	2811	45° S	90° W	South Eastern Pacific
8	1407	58° S	65° W	Cape Horn
9	9843	38° N	60° W	North Western Atlantic
10	8666	20° N	45° W	North Western Atlantic
11	3376	40° S	45° W	South Western Atlantic
12	10299	45° N	30° W	North Eastern Atlantic
13	6984	0	25° W	Tropical Atlantic
15	5162	20° S	0	South Eastern Atlantic
16	3256	40° S	25° E	Cape of Good Hope
17	4744	25° S	55° E	South Western Indian Ocean
18	6480	5° S	65 E	Tropical Indian Ocean
20	7347	5° N	90 E	Tropical Indian Ocean
21	7769	10° N	115° E	South China Sea
24	7785	10° N	160° E	Tropical Western Pacific
25	9972	40° N	180°	North Central Pacific

Table 6.1.3-1 Location of Transit Sites

The metocean conditions at these sites are very varied, covering everything from tropical to extra-tropical and from open ocean to somewhat sheltered.

The MOB is expected to be sailed in an unballasted condition during transit, so these sites are expected to govern strength design in the unballasted configuration, and should be used for estimating fuel use in transit and transit times.

6.2 The Hindcast Data

6.2.1 Hindcasting – The Primary Data Source

After examining potential sources of data for the quantitative specification, it was decided to use data from wind, wave and current hindcasting. Wave and current hindcasting are discussed in Section 5.3.4. The art and science of hindcasting of waves have progressed to the point that hindcast data are now used routinely in the design of many vessels and fixed and floating offshore platforms throughout the world. The following documents the reasons for choosing hindcast data for this project.

Wave hindcasting:

- Hindcasting is not subject to the biases and uncertainties as data from at-sea visual estimates. This is particularly true of open ocean locations, where relatively few long-term accurate wave measurements are available. Because ships try to avoid storms, there is a natural low bias in much of these data that has to be removed by estimating the bias.
- Data can be determined at any site of interest, and are not subject to availability of records.
- Long-term hindcasts over many decades can be made, whereas wave measurements are frequently not available for that long.
- Quite few measured records in the past have included wave directions, while these come automatically with hindcast data.
- Hindcasting can include directional spreading effects not often measured by buoys, or estimated by observers.
- Very little measured data are available in the intense regions of tropical storms.

Current hindcasting:

- Although measurements of currents in coastal and estuarine waters have been made for many years, relatively few deep ocean sites have long-term current data, due to the difficulty and expense of such measurements. Long-term hindcasts over many decades can be made with relative ease.
- Data can be determined at any site of interest, and are not subject to availability of records.
- Very little measured data are available in the intense regions of tropical storms.

Winds:

- Due to the ease of measurement of winds, there are far more reliable wind data, both on land and sea, than exist for waves or currents. However, long-term data may not be available at any site of interest, especially in the ocean.
- Very little measured data are available in the intense regions of tropical storms.

A final reason for adopting hindcast data for this Specification is that it provides concurrent wind, wave and current, and hence allows joint statistical properties to be derived and used.

The hindcasts used in this project come from various sources, as described below:

At all sites, both deployment and transit, winds, waves and currents for about 20 years of hindcasting were obtained from numerical models that cover all the oceans of the world. Using a time interval of 6 hours for winds and waves, and 3 days for currents, these models can be expected to represent large-scale winds, waves and currents well. They would not be good for situations in which the distance between the grid points is not small relative to the scale of the shore profiles, or the wind event scale, or when the rate of change of the environmental conditions is not significantly longer than the time interval used. Thus, these hindcasts are good for open ocean sites, away from complex land details, and for storms that extend over periods of at least a few days, and at least several hundred miles.

The deployment and transit sites are all in the open ocean, so unless a storm has small space or time characteristics, these global hindcasts should produce valid predictions of winds, waves and current.

However, a special problem arises for tropical regions. Tropical areas of the world are subject to typhoons (hurricanes, cyclones) that extend over only a few hundred km, with the intense region being rather smaller than this. Figure 6.2.1-1 shows the principal regions of the world subject to these types of tropical storms. Because of both the time and space scales used in a global hindcast model, and because detailed wind data are not available within the region covered by the typhoon, global hindcasts give only a crude representation of the wind and wave fields during these events.

Typhoons at the Northwest Pacific deployment site are the most intense in the world, exceeding those in the Gulf of Mexico that Americans are most familiar with. The importance of typhoons at this site, and the importance of this site, led us to commission a special study of typhoons at this site, by Oceanweather, Inc., that provided wind and wave data during these typhoons.

Although both the Arabian Sea and the Sea of Japan experience typhoons also, no typhoons were run at those sites, for the following reasons. The Sea of Japan experiences some of the Northwest Pacific typhoons, but due to its more sheltered location, it is unlikely to be more critical than the Northwest Pacific site. The Arabian Sea is open ocean, but typhoons are considerably less severe in this ocean. For this reason, the hindcasts in the Arabian Sea and Sea of Japan should be used with considerable care. Since typhoons may be in the region during several tens of days each year, the data

associated with the most severe 30 days or so is somewhat suspect for accuracy. If these sites are to be considered in any detail, additional consideration should be given to these issues. However, from the point of view of structural design, fatigue damage and operational severity, the North Atlantic and Northwest Pacific sites will clearly provide the most severe general conditions.

No typhoon hindcasts were run at any transit sites, either, although several transit sites are subject to typhoons (i.e., hurricanes or cyclones.) See for instance, Figure 6.2.1-1. Any realistic long-term description metocean conditions in these regions should include careful modeling of typhoons, but it would be impossible to include realistic typhoon hindcasts at all transit sites where major tropical storms occur, for reasons mainly of cost. During transit, the MOB can be expected to skirt around localized intense storms, such as typhoons, so that it may not even be relevant to include typhoon information in transit site data. On the other hand, when deployed, the MOB will have no choice but to ride out such storms, mostly disconnected and in ballasted configuration, so these storms should be considered in the environmental database for any critical deployment site.

6.2.2 Winds

6.2.2.1 Global Winds

The primary wind data are from the NCEP/NCAR CDAS/Reanalysis Project climatology. (NCEP is the National Centers for Environmental Prediction; NCAR is National Center for Atmospheric Research; CDAS is Climate Data Assimilation System. (See Kalnay, Manamitsu et al. (1996)).

Until recently, the meteorological community had to use analyses for weather forecasting that were very inhomogeneous in time as there have been big improvements in the data assimilation systems. This played havoc with climate monitoring as these improvements often produced changes in the apparent "climate". NCEP and NCAR cooperated in a project (denoted "Reanalysis") to produce a 40-year record of global analyses of atmospheric fields in support of the needs of the research and climate monitoring communities. This effort involved the recovery of land surface, ship, rawinsonde (balloon), pibal (also balloon), aircraft, satellite and other data, quality controlling and assimilating these data with a data assimilation over the reanalysis period 1957 through 1996. This eliminates perceived climate jumps associated with changes in the data assimilation system. The database was enhanced with many sources of observations not available in real time for operations, provided by different countries and organizations.

Archives have been created to satisfy different user needs, including one CD-ROM per year containing selected subsets of NCEP/NCAR Reanalysis products for each year that has been processed. Wind data are available at 6-hour intervals for an elevation of 10 m.

These data were obtained by Oceanweather for the years 1974-1996, and used in their wave analyses. A grid spacing of 1.25° in latitude by 2.5° in longitude was used as shown in Figure 6.2.2.1-1 from Oceanweather (1998). Data were provided to the project at the four deployment sites and at the 21 transit sites. It consists of wind speeds and directions.

Note that the meteorological convention is used for directions, that is, the direction is the direction from which the wind blows.

6.2.2.2 Typhoon Winds

Typhoon wind fields were derived for the Northwest Pacific site by Oceanweather, Inc., as part of their typhoon wave hindcast studies. These typhoons were chosen among the 25 most intense at the site during 50 years.

A detailed description of the development of the wind fields is given in the typhoon hindcast report by Oceanweather in Appendix B, and the following is only a brief summary.

The first task was the selection of the 25 typhoons. Using a central pressure threshold requirement of being less than 950 mb, all typhoons that passed within a 2° box, centered on the site, were identified, resulting in a count of 22. (One had "exactly" 910 mb and was not included in the hindcast set.) Then, the exercise was repeated with a 4° box, resulting in 49 storms. With the storms traveling through the boxes, one would expect about twice as many in the 4° box as in the 2° box, and this ratio of 49 to 22 is 2.2. The intensity distribution of these storms was also quite similar for these two cases, as it was also for four more searches using the four 2° boxes that comprise the 4° box. Therefore, it was concluded that the typhoon intensities were quite evenly distributed over the area and the 22 typhoon within the 2° box represented the region well. These were therefore included in the hindcast set. Three supertyphoons, Kit, Flo and Nancy were more severe than any that Oceanweather had ever hindcast, and they decided to include them in the set also, although because of their not passing so close to the site, the associated winds and waves turned out to be not as great as most of the others.

Table 6.2.2.2-1 summarizes the hindcast typhoons.

Name of Typhoon	Max. Hindcast Wave Height at Site (m)	Year	Date
Not named by Oceanweather Called Agnes sometimes	12.8	1948	Nov 15-19
Agnes	13.2	1952	Nov 2-6
June	9.3	1954	Sept 9–13
Alice	13.6	1958	July 18-22
Helen	13.7	1958	Sept 12-17
Tilda	17.6	1961	Sept 29 – Oct 3
Nancy	8.8	1961	Sept 12-16
Karen	11.0	1962	Nov 13-17
Kathy	8.9	1964	Aug 15-22
Wilda	9.1	1964	Sept 21-24
Shirley	9.4	1965	Sept 7-10
Trix	16.5	1965	Sept 14-17
Faye	7.4	1965	Nov 23-26
Kit	4.3	1966	June 25-28
Alice	8.9	1966	Aug 30 - Sept 2
Billie	10.6	1970	Aug 25-29
Ruby	11.1	1976	June 29 – July 3
Therese	10.5	1976	July 14-18
Louise	8.3	1976	Nov 4-7
Elsie	9.6	1981	Sept 28 - Oct 2
Ellis	12.2	1982	Aug 23-26
Kelly	9.4	1987	Oct 13-16
Nelson	14.7	1988	Oct 4-8
Flo	7.2	1990	Sept 15-19
Janis	8.9	1992	Aug 5-8

Table 6.2.2.2-1 Typhoons Hindcast by Oceanweather

The storm tracks for these 25 typhoons (from meteorological records) are shown together in 6.2.2.2-2, from the Oceanweather report in Appendix B and separately in Figures 6.2.2.2-3 through 6.2.2.2-27. In these figures, the Saffir-Simpson Hurricane Intensity Scale is shown by color, as defined in Table 6.2.2.2-2, showing the buildup and decay of the typhoons. All originate in the open sea generally southeast of the site and travel in the generally northwest direction.

Type	**Category**	**Pressure**	**Wind speed**		**Surge**	**Line Color**
		(mb)	(knts)	(mph)	(ft)	
Depression	TD	----	<34	<39	----	Green
Tropical Storm	TS	----	34-63	39- 73	----	Yellow
Typhoon	1	> 980	64- 82	74- 95	4- 5	Red
Typhoon	2	965-980	83- 95	96-110	6- 8	Light Red
Typhoon	3	945-965	96-112	111-130	9-12	Magenta
Typhoon	4	920-945	113-134	131-155	13-18	Light Magenta
Super Typhoon	5	< 920	> 134	> 155	18	White

Table 6.2.2.2-2 Saffir-Simpson Scale for Typhoon Intensity

Working from available historical data sources including aircraft reconnaissance data, ship and buoy reports, weather maps, and annual cyclone reports produced by various agencies the following cyclone parameters were developed:

- Storm track
- Time history of central pressure, peripheral pressure and ambient pressure gradient
- Radius to maximum wind

From the selected typhoon parameters, using procedures documented in Appendix B, the wind fields were developed within a region from 10° N to 35° N, and from 120° E to 150° E, as shown in Figure 6.2.2.2-28. The grid spacing was 0.225° in latitude and 0.2497° in longitude. Results were archived at 1-hour intervals. They consist of wind speeds and directions. Note that the meteorological convention is used for directions, that is, the direction is the direction from which the wind blows.

Results were archived for the project over an area about 10° x 10°, (approximately 650 miles square) as shown in Figure 6.2.2.2-29. The purpose of this was twofold.

Firstly, it allowed the statistics from the typhoon hindcasts to be expanded somewhat, giving considerably more accurate data than would have been found from the wind and waves at just the site itself. The reason for this is as follows.

From the study of the typhoon geographical distribution, it was found that typhoons passing within about 2° of the site had very similar intensity distributions, there being no preferential routes. Therefore, by looking randomly at hindcast data at a variety of sites in the region, we are essentially allowing the 22 typhoons to have passed randomly along different tracks within the region. As seen by the relatively small wind speeds and wave heights at the site from the three supertyphoons that passed through the 4° but not the 2° box, Kit, Flo and Nancy, there was no need to include a wider region than about 2°, for, outside that region, even these very intense typhoons had little impact at the site, compared to smaller ones within the 2° box. Section 6.6.5.4 describes one method of processing the hindcast data to realize this feature. Typhoons Kit, Flo and Nancy could be included in similar processing, by using a box centered around the region they passed through.

The second reason for saving the data over a large region of the ocean was to use in the event study of several typhoons, as described in Section 6.7.

6.2.3 Waves

6.2.3.1 Global Hindcasts

The global wave hindcast was performed by Oceanweather using the wind field histories described in Section 6.2.2.1. The hindcasting is described in detail in Appendix A, and the following provides a summary.

The hindcast model was the so-called ODGP2 spectral wave model. This model consists of the deepwater ODGP2 growth-dissipation algorithm, coupled with a global wave propagation system with great circle propagation effects included. The grid spacing of 1.25° in latitude by 2.5° in longitude was used as shown in Figure 6.2.2.2-1 from Oceanweather (1998). The model uses a directional wave spectrum consisting of 24 directions and 15 frequencies.

Wind fields were derived from the NCEP/NCAR CDAS/Reanalysis Project climatology updated at 6-hourly intervals, the model time step was 3 hours, and wave data were archived at 6 hours. The years covered are from 1974 through 1996. Data were provided to the project at the four deployment and 21 transit sites.

The wave data that were archived are listed in detail in Appendix A, and the following is a summary of relevant sections:

To reduce the amount of archived data to a manageable amount, the 24 x 15 matrix representing the wave spectrum at any location was reduced to a set of 21 parameters. These parameters contain the wind speed and direction and sets of variables that describe the waves in various ways.

The first characterization of the waves gives considerable detail of the total spectrum. It provides the significant height, Hs, and, redundantly, the variance, ETOT, (where ETOT = $H_s^2/16$), the peak spectral period, TP, the vector mean direction, VMD, the first spectral moment, M01, and the second spectral moment, M02. The peak period and the two moments allow a rather detailed description of the frequency distribution, but no information is provided on the directional spreading with this characterization, and some assumption would have to be made about this independent of the data.

If desired, more information can be used on directionality if either of two other characterizations is used. In each, by comparing the wave spectrum and the wind strength, a part of the directional spectrum is extracted that represents the "sea", the part of the spectrum that is caused by the wind blowing over the ocean at the location itself. After extracting the sea, the balance of the spectral energy is defined as "swell", the waves formed by winds elsewhere in the ocean that propagate to the location.

In the first of these characterizations, the seastate is defined by one sea train and one swell train, each being defined by its variance (or significant height if the relation given above is used), the peak spectral period and the vector mean direction.

In the second characterization, two swell wave trains are used in addition to the sea.

These last two types of data contain more information on wave directions than the characterization by one spectrum, but give less information on frequency content. It is generally recommended that the characterization with sea and two swell trains be used.

6.2.3.2 Typhoon Hindcasts

These hindcasts were made using the wind fields described in Section 6.2.2.2. The same wave model was employed by Oceanweather, Inc.

The region covered by the hindcast was from 10° N to 35° N, and from 120° E to 150° E, as shown in Figure 6.2.2.2-28. The grid spacing was 0.225° in latitude and 0.2497° in longitude, with at time step size of 30 min. Results were archived at 1-hour intervals. The wave model was the same as for the global hindcast, using a directional wave spectrum consisting of 24 directions and 15 frequencies. As for the wind field, the waves were archived over a region about 10° square, as shown in Figure 6.2.2.2-29.

The wave spectrum can be characterized by the total spectrum, just as for the global wave hindcast, the data being archived being Hs, and, redundantly, the variance, ETOT, (where ETOT = $H_s^2/16$), the peak spectral period, TP, the vector mean direction, VMD, the first spectral moment, M01, and the second spectral moment, M02.

In addition, two variables are given to provide a measure of the angular spreading.

The variable called ANGSPR is provided to describe the angular spreading. This is the mean value over the 552 bins for direction and frequency of the calculated spectrum of $\cos(\theta\text{-VMD})$, weighted by the variance component in each bin. If the angular spectrum is uniformly spread over 360°, this statistic is zero; if uniformly spread over 180°, it is $2/\pi$,

and if all the variance is concentrated at the VMD, it is 1. For the use of this variable in fitting an exponential distribution to the angular spectrum, see Pearson and Hartley (1976).

Another measure of directional spreading is provided, called INLINE. This is the ratio of the inline to total wave energy, defined by Haring and Heideman (1978) as:

$$\text{INLINE} = E_T(\theta_d) / \Sigma E(\theta_j) \qquad (6.2\text{-}1)$$

Where $E_T(\theta_d)$ is the total wave energy in the dominant direction due to waves propagating in all directions, and is given by:

$$E_T(\theta_d) = \Sigma E(\theta_j) \cos^2(\theta_j - \theta_d) \qquad (6.2\text{-}2)$$

where θ_d is the dominant wave direction.

Instead of using these measures of angular spreading, the spectrum is broken up into wind sea and swell, as described for the global wave hindcast, with one sea and one swell component.

6.2.4 Currents

Current data came from three independent hindcasts. Each hindcast contributed data not available in the others. The three are: global model currents, local wind-driven currents model, tidal currents model.

Unlike for winds, there are no operational products that provide upper ocean currents on a regular basis. The climatological data, based on ship drift and/or surface drifters, are not well suited for engineering and design purposes due to their low spatial and temporal resolution. A better source of current data is one that produces realistic time series for use in simulations and from which statistics can be computed.

Our recommendation is to create such a database by combining a global ocean model hindcast with hindcasts of local tides and wind-driven flow. The advantages of the global model are that it does a fair job of creating the general circulation from a physics-based model forced by the global wind field and that its use allows ocean current time series to be selected from a model grid point close to the desired site. Disadvantages of the ocean model and the sources of uncertainties, if it were to be used alone, are that:

1) Its basic ~3 day time step does not resolve the near-inertial response of the ocean over much of the globe;

2) Its lack of vertical structure near the sea surface and lack of heat and freshwater flux forcing results in unrealistic surface mixed-layer depths and as a result, unrealistic wind-driven flow;

3) That it lacks tidal currents; and

4) That it does not in all regions replicate the strength of the ocean flows.

Our recommendation is thus to adjust the model currents and add to them time series of the local tides and wind-driven flow. By comparison with observed upper ocean time series, we believe this to be an approach that minimizes the uncertainties in the hindcasts of currents.

The spectra of observed currents at the instrumented buoys discussed in Appendix G also show spectral peaks associated with tides. Because of the 3-day sampling interval and because it lacks the appropriate physics, the global ocean model does not produce tides. Because tides are an evident spectral peak, with regional variability in, for example, the strength of the diurnal versus semi-diurnal tides, we have chosen to use a model developed to predict global tidal currents to add a time series of tidal currents.

6.2.4.1 Global Current Hindcast

The first hindcast was provided by the Oceanography Division of the Naval Research Laboratory (NRL). The current model uses winds to compute the shear forces on the ocean surface and hence, from dynamic equations of equilibrium, the currents in the ocean. The model used was driven by winds from European Center for Medium Range Weather Forecasts (ECMWF), (ECMWF (1998)). The model assumes constant density, and there are no mixed layer effects included. However, it is sophisticated enough to resolve the effects of large eddies in the ocean.

The model covers all the oceans of the world with a $^{1}/_{16}$ degree grid spacing, and was run over the years 1979 to 1996. The model has six layers in the vertical direction, but as the MOB has a draft of only about 100 ft, the information relevant to the MOB is in the upper layer, which is typically 300 ft in thickness. The current speed and direction were archived at 3.05 day spacing, at the grid points nearest to the four deployment sites and the 21 transit sites. In addition, to enable comparisons between the hindcast currents and measurements at deep ocean buoys, current data were obtained at another 8 sites at various locations around the world.

These current data were supplemented by local wind-driven currents computed by BNI from the NCEP/NCAR CDAS/Reanalysis Project winds at 6-hourly intervals, as described in the next section.

Due to the awkward time interval of 3.05 days, and the archiving of data in non-calendar years, the original data from NRL were re-organized into annual archives at 3.0-day intervals using interpolation.

6.2.4.2 Local Wind-driven Current Hindcast

The NRL global model, covering the whole ocean, provides good modeling of large-scale processes, such as the effects of winds that blow over long periods of time and produce currents that move thousands of miles. The time step size of 3.05 days (converted to 3.0 days for this Specification) allows effects that occur over many days or months to be modeled. However, there was no attempt to model events that occur within a shorter time scale. Once such class of events is the current that is produced locally from the wind.

A conceptual model of the complete current distribution would be of an ocean where the surface mixed layer is free to move relative to the interior, essentially "sliding" over the interior at the bottom of the mixed layer. The interior has a velocity field that is basically geostrophic. That geostrophic flow continues to the surface, but in the surface layer there is the additional local wind-driven flow. The most energetic part of that wind-driven flow is likely to be the near-inertial oscillations. The wind-driven flow speed is inversely proportional to the mixed layer depth so we need to know the depth of the mixed layer to model these currents.

The local inertial period is 0.5/(sin (latitude)) days, so everywhere poleward of about 8° the local inertial period is shorter than 3.05 days, and so would not be modeled at all by the global current model.

The inertial currents are very sensitive to the time history of the wind vector at the point of interest. They are the resonant response of the ocean, where that resonant response is a clockwise (counterclockwise) rotation of the currents at the inertial period in the northern (southern hemisphere). If, at the point of interest, the wind turns with the inertial period in the direction of the inertial response, it will be exceptionally capable of generating large surface currents. The rotation rate and direction of the wind at a fixed point as a typhoon passes depends on the location of the point relative to the typhoon track and the rate at which the typhoon translates across the sea surface. Pick the right quadrant of the typhoon and set the translation speed of the typhoon just right, and the surface winds will turn with the inertial currents and excite extremely large such currents.

A more complete description of the inertial and lower frequency currents can be based on the addition of a surface layer current from local wind effects to the global NRL results. Two models were used. The first was used in predicting currents from global winds at the global sites. The second was used for typhoon-driven winds at the Northwest Pacific Site.

The model used for global winds at the deployment and transit sites was based on the following formula:

$$\begin{aligned} \partial u/\partial t - f_c v &= (1/\rho_w D)\tau_x - cu \\ \partial v/\partial t + f_c u &= (1/\rho_w D)\tau_y - cv \end{aligned} \qquad \text{(6.2-3, 6.2-4)}$$

where: u, v are horizontal velocity components in x, y directions, respectively,

f_c is the coriolis parameter,
t_x, t_y is the wind stress vector,
c is a damping coefficient that was chosen as 1/5days, and
r_w is the water density, and

D is the mixed layer depth

Since these differential equations are functions of time only, at a given site, and are not dependent on wind or current at adjacent sites, they can be solved at a site with no knowledge of adjacent regions. The mixed layer depths were estimated for each month from oceanographic data in the World Ocean Atlas 94, and the appropriate values were used in solving the equations. These mixed layer depths are summarized in Appendix I. The time step size for each was one hour, to resolve inertial periods.

The wind input for the solution came from the wind data archived by Oceanweather for the global hindcast. Since the time step for winds was 6 hours, the wind was held constant during this 6 time steps between wind data values. To enable comparisons of these hindcast currents with measured data, currents were also computed from measured winds at 8 sites around the world where instrumented buoys were deployed.

An initial attempt at using the above equations 6.2-3, 6.2-4 for the typhoons at the Northwest Pacific site resulted in currents that were unreasonably high. The reason for this was that, during the late summer and fall, this site has quite a shallow mixed layer, but, during typhoons, it gets stirred up by the high shear stress at the bottom of the layer, and by the large waves that accompany the high winds. As a result, the mixed layer becomes considerably deeper during typhoons, a characteristic that is not modeled by these equations. For this reason, the currents were then re-computed using the first model described in Section 5.3.4.2. This model, referred to as the PWP model, has been verified against observations (Figure 5.3.4.2-1) and adapted by the U.S. Navy for predicting the penetration depth of the diurnal mixed layer and sea surface temperatures.

The program allows the depth of the mixed layer to change as a result of the mixing process and accepts a heat flux into the water at the air/sea interface. This flux was set to zero for these calculations, due to the short time the typhoons that were present. It uses a temperature and salinity profile with depth to initiate the computation. From these profiles the mixing calculations are performed, and the mixed layer depth is computed by the program at each time step. Initial runs indicated that there were some significant oscillations in the predicted currents when a time step of one hour (the time intervals for the typhoon hindcasts) was used. The program was therefore modified so that it read time steps at one hour spacing but performed the computations with a smaller time step. This considerably improved the smoothness of the results. The PWP program was also modified to accept the format of the typhoon winds from the Oceanweather hindcasts, for successive typhoons. In the absence of other information the currents were initialized at zero at the first hour or the typhoon provided buy Oceanweather. The resulting program is called PWPMOB. A listing of the program is given in Appendix D.

6.2.4.3 Tidal Currents

Tidal currents, although not very large in the open ocean, do exist, and since their major components have periods of about 12 hours, these will not be resolved in the NRL model. Tidal currents were obtained from a model developed by Dr L. Kantha (1995) at the four deployment sites. This project was a joint effort between University of Colorado / Colorado Center for Astrodynamics Research (CU/CCAR), Mississippi State University / Center for Air Sea Technology, (MSU/CAST), and the U.S. Naval Oceanographic Office (NAVOCEANO).

This model is a barotropic model; that is, it uses a vertically-averaged component of the motion. This is considered reasonable for most purposes.

Tidal currents are caused by the gravitational attraction of the moon (and sun), together with the centrifugal forces from the rotation of the earth and moon about their center of mass. For this reason, the currents can be described by a series of harmonic motions of various periods, amplitudes, phases and directions. There are several components of tides that are important: the semi-diurnal tides (i.e., M2, S2, N2 and K2), with roughly two tidal cycles every day; diurnal tides (K1, O1, P1 and Q1), with roughly one tidal cycle per day and the long term tides (such as the MF, MM and SSA), which are fortnightly, monthly and semi-annual in nature. Figures 6.2.4.3-1 and 6.2.4.3-2 show a global view of two such harmonics, known as K1 and M2.

The tidal currents were extracted from the global model at the four deployment site only. Due to the small magnitudes and short periods of tidal currents, it was not considered necessary to request currents at the transit sites.

Table 6.2.4.3-1 gives the components at these sites.

Harmonic	Northwest Pacific	North Atlantic	Arabian Sea	Sea of Japan
Magnitude (cm/sec)	2.9	1.4	1.4	1.0
Dominant Direction	East-West	No dominance	North-South	North-South

Table 6.2.4.3-1 Tidal Current Components at Deployment Sites

6.3 Inclusion of Environmental Effects not Present in Hindcast Data

The hindcast data described in Section 6.2 are expected to give reliable long-term statistics that can be used in the design of the MOB. However, considerable detail in both time and space is missing from these data due to the nature of the hindcasts. For instance, the wind provided in the hindcasts is the 1-hour wind at elevation 10m. If an element of the MOB is being designed on the deck, the analyst will want to know the 1-hour mean wind at this

elevation, and perhaps the changes in wind speed that occur from turbulence in the air flow. To complete the environmental description, Section 6.3 describes many environmental characteristics that may also be used in the design of the MOB. These vary from including turbulent variations of wind speeds, defining the spectral shape for wave spectra and providing the vertical current profile. Table 6.3-1 summarizes the issues discussed in this section. Internal waves are also included in this section.

Wind	Waves	Global Current	Wind-driven Current
Wind speed spectrum	Spectral shape	Variation of speed and direction with depth	Variation of speed and direction with depth
Vertical velocity profile	Directional spreading shape	Spatially rapid changes in speed from oceanic fronts	
Lateral horizontal variations	Nonlinearities especially coherence		
Longitudinal horizontal variations			
Rapid changes in speed and direction from atmospheric fronts			
Rapid Changes in Direction			

Table 6.3-1 Information not Included in Hindcast Data

6.3.1 Wind

Wind speed information obtained by direct measurement or developed by hindcasting usually consists of peak gust (i.e., 2 s to 3 s gust), one-minute, or mean hourly speeds at a standard elevation, e.g., at 10 m or 20 m above the mean water surface. The wind speed field in the atmospheric boundary layer is not uniform in space and time. For this reason, information is needed on vertical mean wind profiles, horizontal variation of the mean speeds, spectra of velocity fluctuations (describing turbulent fluctuations at one point), and cross-spectra of velocity fluctuations (describing the spatial structure of the turbulence). These issues are dealt with in Sections 6.3.1.1 to 6.3.1.3.

6.3.1.1 Vertical Variation of Mean Wind Speed

Vertical mean speed profiles provide a basis for estimating the variation of mean wind forces as a function of elevation within the surface atmospheric sublayer. For all strong winds - except possibly waterspouts, about whose flow structure little is known - it is

permissible to model the vertical mean wind speed profile by the logarithmic law, defined by equations 6.3-1 and 6.3–2.

$$U(z) = U(10)\ \ln(z/z_o)/\ln(10/z_0) \qquad (6.3\text{-}1)$$

U(z) denotes the mean wind speed averaged over one hour at elevation z,
z_o is the roughness length, which is often taken as $5x10^{-3}$ m for flows over the ocean, but for winds between 4 m/sec and 20 m/sec it should be computed (in meters) from equation 5.2.2, rewritten here as equation 6.3-2.

$$z_o = 10\ \exp\{-17.7\ [U(10)]^{-0.23}\} \qquad (6.3\text{-}2)$$

where U(10) is the mean wind speed in m/sec at 10 m above the mean water level. For winds over 20 m/sec, use the value of z_0 at 20 m/sec, namely $z_0 = 1.38x10^{-3}$ m.

It is of interest to see how much variation there would be over 45 m, the approximate height of a MOB. Assuming a mean wind speed at 10-m elevation is U(10) = 20 m/s, we get the following results.

Elevation (m)	1.0	10.0	45.0
Speed (m/sec)	14.8	20.0	23.4

So the wind speed at the deck is about 20% higher than the hindcast value at 10 m, a significant amount considering that wind forces vary as the square of the speed.

6.3.1.2 Horizontal Variation of Mean Wind Speed

Large-scale Storm Systems

For large-scale storm systems, it may be assumed that the mean wind speed does not vary significantly along the MOB in a horizontal direction normal to the mean speed direction. This is true even for a storm system as small in dimensions as a tropical cyclone.

To show this, consider the example of a MOB subjected to wind speeds associated with a tropical cyclone. For simplicity we assume that the tropical cyclone's translation velocity, V_f, is negligible, the radius of maximum wind speeds is R_m = 10 km, the latitude is 25^0, the maximum tropical cyclone hourly mean wind speed at 10 m elevation is 40 m/s, the length of the MOB is 1.5 km, and the longitudinal axis of the MOB is normal to the tangential velocity of the tropical cyclone vortex. Let the radial distance from the vortex center be

denoted by r. The distances between the center of the storm on the one hand and the near and far end of the MOB on the other are, respectively, 9,250 m and 10,750 m.

The gradient wind speed at radius r may be modeled by the following equation (Gradient winds are winds above the atmospheric boundary layer, where surface friction effects are negligible).

$$V_{gr} = - rf_c /2 + [(rf_c /2)^2 + (r/\Delta)\delta P\, R_m\, e^{-Rm/r}/r^2]^{1/2} \qquad (6.3\text{-}3)$$

where

Δ is the specific mass of air,
δP is the difference between the atmospheric pressures at the center of the tropical cyclone and at the outer limit of the tropical cyclone wind field
f_c is the Coriolis acceleration , equal to $0.6164 \times 10^{-4} s^{-1}$ at this latitude.

For R_m=10 km, from Eq. 6.3-3 we obtain the following mean hourly gradient speeds over the near end and the far end of the MOB, respectively: $V_{gr,far}$=39.95 m/s and $V_{gr,nr}$=39.91 m/s. The corresponding speeds at the 10 m elevation may be modeled by Eq. 5.2-4, that is, by multiplying the gradient speeds by the factor 0.865 (recall that we assumed s=0). It is seen that the theoretical differences between the wind speeds at the two ends of the 1.5 km long MOB are very small – undoubtedly considerably smaller than the deviations of the actual speeds from the model used in this example.

Since most tropical cyclones have radii of maximum wind speeds considerably larger than 10 km, it may be expected that the horizontal variation along a MOB of rotational wind speeds in large-scale storms is negligible for practical purposes in most cases.

Note, however, that speeds vary temporally about the mean, and that this temporal variation is non-uniform in space. This non-uniformity in time and space may affect the design of a MOB or parts thereof - see Section 6.3.1.3.

Cold Fronts

A cold front has a rapidly changing wind speed and direction. The following explores possible effects of such events.

There do not currently appear to be readily available statistical data on the rates of change of wind speeds during the passage of a front. The values assumed here for the translation velocity and the wind speed represent very rough estimates by competent meteorologists, rather than hard values based on measured data. For the purposes of design, it could be assumed that the front moves at a speed of about 10 m/sec with winds within the front blowing at a similar speed. In addition, it is noted that cold fronts are in reality non-uniform along their length, resulting in non-uniformities in the wind speeds, for which no quantitative data appear to be available.

It was noted in Section 5.2.1.3 that few empirical data or statistical studies on the time rate of change of the wind direction are available. For design purposes it may be assumed tentatively that, for both moderate and strong winds, the rate of change rarely exceeds 1°/sec, and that on average it is lower than 0.25°/sec.

If a front were to hit a MOB whose long axis is not parallel to the front, the front will hit the upwind module before the downwind module, loading the modules unevenly with winds whose speeds and directions are rather different, and creating internal forces in the connectors or a need for dynamic positioning. A crude estimate of possible effects of a cold front follows.

Consider a cold front advancing with translational velocity of 10 m/sec toward a 1.5 km long MOB, making a 45° angle with the longitudinal axis of the MOB. The differential time between arriving at the two ends is

$$\delta t = [1{,}500 \text{ m} / (2)^{1/2}] / (10 \text{ m/s}) \approx 100 \text{ sec.} \qquad (6.3\text{-}4)$$

By the time the right end has been hit by the front, the speed at the left end will have veered by an angle of, say, 100 sec x 0.25°/sec = 25°. Thus not only is there a difference of wind speed at the two ends, but the directions of the wind at the two ends differ significantly, causing a bending moment in the horizontal plane.

Thunderstorms and Waterspouts

Non-uniformities of the wind speed affecting a MOB can be more significant for smaller-scale storm systems like thunderstorms (Simiu and Scanlan (1996), p. 28) or waterspouts. Where local effects caused by waterspouts are of concern, calculations similar to those presented in the example of the section “Large-scale Storm Systems” are warranted. At present, statistical information available to structural engineers on the occurrence and spatial properties of thunderstorms is limited. Even less information is available for waterspouts, although it is commonly believed that they are considerably weaker than tornadoes. Nevertheless, Dr. Joseph Golden, Senior Meteorologist, Office of Atmospheric Research, NOAA (e-mail JoeG@oar31.oar.noaa.gov) has information on a waterspout that occurred near China with intensity that was estimated to have winds of over 200 mph, and caused significant damage on a ship. Since no better information is available, the following crude model for the tornado tangential velocity U has been used in applications:

$$U = (r/R_m)\, V_m \qquad (0 < r < R_m) \qquad (6.3\text{-}5)$$

$$U = (R_m/r)\, V_m \qquad (R_m < r)$$

where V_m is the maximum tangential wind velocity and R_m is the radius of maximum rotational wind speed (see Simiu and Scanlan (1996), p. 127). Radial and vertical velocities in a tornado have been assumed in applications to be one-half (directed inward) and two-thirds (directed upwards) times the tangential component, respectively (see Simiu and Scanlan (1996), p. 583).

6.3.1.3 Turbulence: Integral Scales, Spectra, and Cross-spectra of Velocity Fluctuations about the Mean

Longitudinal turbulence fluctuations and/or vertical turbulence fluctuations may be important for the design of long-span, flexible structures. The longitudinal and vertical integral turbulence scales are of the order of 700 m and 350 m, respectively (see Eq. 5.2-5 and the text following that equation). For example, an individual vertical eddy covers only a portion of a MOB, and would be essentially uncorrelated with an adjacent vertical eddy.

For quantitative purposes it is useful to consider the spectra and cross-spectra of the longitudinal and vertical velocity fluctuations.

The following expression may be used for the spectrum of the longitudinal velocity fluctuations in the high frequency range (i.e., for $fz/U(z)>0.2$), where f = frequency (Hz) and z = elevation):

$$S(z,f) = C\, z\, U(z)/\{[2.5 \ln (z/z_o)]^2 [1 + D\, f\, z/U(z)]^{5/3}\} \qquad (6.3\text{-}6)$$

where $C = 200\beta/6$, $\beta = 6.5$, and $D = 50$, and z_0 has been previously defined in equation 6.3-2.

For low frequencies ($fz/U(z) < 0.01$) the von Karman spectrum may be used:

$$S(z,f) = 4\, \beta\, L_u^x\, U(z)/\{[2.5 \ln(z/z_o)]^2 [1 + 70.8 (f\, L_u^x/U(z))^2]^{5/6}\} \qquad (6.3\text{-}7)$$

where L_u^x is the longitudinal turbulence scale given by Eq. 5.2-5.

For intermediate frequencies ($0.01 < fz/U(z) < 0.2$), S(z,f) may be computed by interpolating between the values that would be found using equations 6.3-6 and 6.3-7.

Spectra of vertical velocity fluctuations are described by Eq. 6.3-6 in which C=15 and D= 9.5.

Cross-spectra of longitudinal velocity fluctuations are described by Eq. 5.2-6. It is reasonable to assume that the cross-spectrum of the vertical velocity fluctuations is given by an expression similar to Eq. 5.2-6, wherein the right-hand side is multiplied by the factor 0.5. This factor is consistent with the fact that the integral vertical turbulence scale is about half as large as the integral longitudinal turbulence scale.

Example

We provide a numerical example of the use of Eqs. 6.3-6 and 6.3-7.

Let z = 30 m and U(z) = 20 m/s. Then from equation 5.2-2, $z_o = 1.38 \times 10^{-3}$ m. From Eq. 5.2-5,
L_u^x = 700 m. Finally from Eq. 6.3-6, for f = 0.5 Hz, we get S(z,f) = 0.474 m^2/sec, and from equation 6.3-7, for f = 0.05 Hz, we find S(z,f)=6.58 m^2/s.

The example shows that the spectral density is higher at low frequencies than at higher frequencies (i.e., frequencies such that fz/U(z)>0.1). Some widely used spectral models fail to reflect this increase, and are therefore inappropriate for use in the design and assessment of very flexible structures.

Note again that the procedures and results discussed in this section pertain to wind speeds considered without regard for directionality.

6.3.1.4 Mean Wind Speeds at Averaging Intervals Less than 6 hours

The basic wind data is provided in this Specification as 6-hourly mean values. For time periods less than that, the following approximate formula is suggested. This formula (API RP2T (1987)) was suggested, in the absence of further information, for converting maximum wind speeds over averaging periods between 3 sec. and 1 hour, but the extrapolation to cover 6 hours only represents a 6% further change in α. Figure 2.3.10 in Simiu (1996) shows approximately the same values.

$$W(t) = \alpha\, W(6)$$

W(t) is the maximum wind speed averaged over time t, and W(6) is the wind speed averaged over 6 hours. α is a function of t, as given in the following table:

Time Period	α
6 hours	1.00
1 hour	1.06
10 min	1.12
1 min	1.25
15 sec	1.33
5 sec	1.39
3 sec	1.41

It is recommended in Section 6.8.3, however, that further research be made to determine wind speed and direction variations and means for periods less than 6 hours.

6.3.2 Wind Waves

The wave hindcasts provide most of the information needed to establish the wave environment for the MOB. These hindcasts are firstly given as a total spectrum with certain parameters describing the frequency and directional distribution. They are also provided as a set of wind waves and swell components, each defined by direction, significant wave height and peak spectral period. It is recommended that the latter be used.

The statistics of extreme waves and hence extreme responses of the MOB can be developed from the data given here. These predictions will be accurate provided that the extreme waves are part of the population modeled here. There has been some speculation and some reasonably hard evidence that "freak" waves, somewhat larger than those expected for a given sea, exist. If this is so, they could be of concern in the design of the MOB. However, it is state of the practice to ignore these waves in the design of ships and offshore installations, and expect the inherent safety factors to guard against failure in these circumstances. For this reason, we are not making any recommendations on the characteristics of freak waves.

6.3.2.1 Spectral Shape

The recommended spectral shape is derived from the DHH (Donelan et al. (1985)) spectrum, as defined in Section 5.2.3.3, and shown again below.

For the range $0.2 < A_w < 1.2$, the DHH spectral form is given by:

$$S(f) = ag^2(2p)^{-4} f^{-4} f_p^{-1} \exp\left[-\left(\frac{f_p}{f}\right)^4\right] g^{\exp\left[-(f-f_p)^2/2m^2 f_p^2\right]} \qquad (5.2\text{-}14)$$

Where:

$$\alpha = 0.006 A_w^{-0.55} \qquad (5.2\text{-}15)$$

$$m = 0.08\left(1 + 4A_w^{3}\right) \qquad (5.2\text{-}16)$$

$$g = 1.7 - 6.0 \log A_w : for\, 0.2 < A_w \le 1 \qquad (5.2\text{-}17)$$

$$g = 1.7;\ for\, 1 < A_w < 1.2 \qquad (5.2\text{-}18)$$

f is the frequency (Hz) and f_p is its value at the spectral peak = $1/T_p$. The spectral parameters (a, m, g) are functions of the wave age A_w only.

This is a modified-JONSWAP spectral form that incorporates the correct (f^{-4}) tail, and includes peak enhancement that depends on the wave age. The wave age A_w is defined from the wind speed and the (phase) speed of the waves (or celerity) corresponding to the peak spectral period, T_p.

$$A_w = C_p/U \qquad (6.3\text{-}8)$$

In general the wind and wind sea will not be in the same direction, so the component of the wind in the direction of the waves should be used to compute the wave age.

In deep water the wave celerity C_p can be found from the relationship:

$$C_p = g\,T_p/(2p) \qquad (6.3\text{-}9)$$

Where: g = acceleration from gravity

This spectral form depends only on the peak frequency and wave age, relaxes to the Pierson-Moskowitz spectrum (except for the slower fall-off of the tail) at full development and appears to describe actively wind-generated waves accurately.

6.3.2.2 Directional Spreading

The recommended directional spreading is modeled by the sech^2 function, as defined in Section 5.2.3.4, the argument of which is parameterized in terms of the ratio of frequency to peak frequency.

$$f(f,q) = \frac{1}{2} S(f) b \sec h^2 b\left(q - \bar{q}(f)\right) \qquad (5.2\text{-}19)$$

Where: $\bar{q}(f)$ is the mean wave direction and b, the spreading parameter, is given by:

$$b = 2.61\left(\frac{f}{f_p}\right)^{1.3};\ for\ 0.56 < \frac{f}{f_p} \le 0.95 \quad (5.2\text{-}20)$$

$$b = 2.28\left(\frac{f}{f_p}\right)^{-1.3};\ for 0.95 < \frac{f}{f_p} < 1.6 \quad (5.2\text{-}21)$$

$$b = 1.24;\ \ otherwise$$

6.3.2.3 Global Hindcasts

The three-component description of the waves can be used to define a directional spectrum, as follows:

Wind Sea

From the wind speed, U, and the spectral peak period, T_p, determine the wave age, A_w. Compute the DHH spectrum with sech^2 spreading to determine the directional wave spectrum.

Compute the DHH significant wave height corresponding to this spectrum from the volume under the spectrum:

$$m_0 = \int \int f(f,q)\,df\,dq \quad (6.3\text{-}10)$$

and

$$H_s = 4\ m_0^{0.5} \quad (6.3\text{-}11)$$

Then, scale the DHH spectrum so that the resulting significant height is 25% higher than the value given in the Oceanweather hindcast.

This adjustment of +25% to the significant height of the wind sea is required to account for the loss of wind sea to swell in the bin-by-bin adjustment to the P-M spectrum. (An equivalent amount of elevation variance will be taken from the swell partition, as described below.) The Oceanweather hindcast of the wind sea is always low because of the criteria used to admit spectral energy to wind sea in any bin, viz. the energy in that bin must not exceed the Pierson-Moskowitz limit. The energy can, of course, be lower, so on average the wind sea energy (or significant. height) is lower than the Pierson-Moskowitz fully developed limit. The average value of the ratio ($g\ H_s / U^2$) is 0.2245 for the 4 deployment sites in full development conditions in the Oceanweather data (see paragraph on page 8 in

Appendix H), while the empirical result from DHH is 0.285. Thus a correction should be used from the ratio 0.285/0.2245 = 1.27, resulting in the upward adjustment of 27%, rounded to 25%. Assuming that the total energy is hindcast correctly, the 25% missing from the wind sea must have been erroneously put into the 2 swell bins. Thus it is recommended that 12% be removed from each of the swell bins.

Swell

No generic spectral shape for swell has yet been determined. Probably none is possible since swell is determined not only by the conditions of its generation but also by the conditions encountered in its passage from its generation area (as wind sea) to the target area being considered. This passage may include much of the large ocean basins and several meteorological systems. However, some generalizations are possible:

The frequency distribution in a swell spectrum is narrower than that of a wind sea. The OWI hindcasts give a mode spectral width (equation 8, Appendix H) of 0.25. The following are the recommendations for spectral shape:

The spectrum for each of the two swell wave trains can be modeled with a DHH spectrum with the following parameters:

A_w = 1.2 (fully developed seas)

a = 0.0054 (corresponding to A_w = 1.2)

m = 0.63 (corresponding to A_w = 1.2)

g = 21 (high peak enhancement factor to force narrow spectrum)

The directional spreading of swell depends essentially on the size of the storm (or that part of it in which swell is generated in a direction towards the target area) and its distance from the target area. The directional resolution of the OWI hindcast model, and indeed of all operational global numerical wave models, is insufficient to provide any guidance here. A rough guide to the total width of the swell is the angular arc subtended by the source area (i.e., the relevant parts of the distant storm) at the target area. In the absence of other information, it is recommended that no directional spreading be used for each swell component.

Finally, scale the DHH spectrum of each of the two swell trains computed above, to give the hindcast significant wave height, reduced by 12.5%, to account for the loss of wind sea to swell in the bin-by-bin adjustment to the P-M spectrum

6.3.2.4 Typhoon Hindcasts

The two-component description of the waves can be used to define a directional spectrum, as follows.

Wind Sea

Repeat the procedure suggested for the global hindcast.

Swell

Repeat the procedure suggested for the global hindcast, with a 25% reduction in the significant wave height. This is because there is only one swell component provided in the typhoon hindcast data, whereas there were up to two given in the global hindcast data.

Nonlinearity

Nonlinearities determine the excess crest heights above mean water level compared to the trough depths. The best way to estimate how important nonlinearity can be in crest heights and wave orbital kinematics would be to run fully nonlinear simulations of two-dimensional wave trains having the spectral shapes and spreading discussed above.

As a preliminary check, the following procedure is suggested, based on checking the largest waves for nonlinearity.

From the total significant wave height, estimate the maximum individual wave in a 3-hour seastate from $H_{max} = 1.9\ H_s$.

Estimate the corresponding most probable individual wave period, from equation 5.2-33.

$$t_m = 2\left(1 + \left(1 + 32n^2 / H_{\max}{}^2\right)^{\frac{1}{2}}\right)^{-1} \qquad (5.2\text{-}33)$$

For this equation the spectral width, ν, can be estimated from equation 5.2-32.

$$n = \left(\frac{m_o m_2}{m_1^2} - 1\right)^{\frac{1}{2}} \qquad (5.2\text{-}32)$$

where m_r are the moments of the frequency spectrum S (f)

$$m_r = \int_o^\infty f^r S(f) df \qquad (5.2\text{-}24)$$

Finally, test for nonlinearity, (Shore Protection Manual (1984)) by seeing if

$$H_{max}/(g\tau_m^2) > 0.007 \qquad (6.3\text{-}12)$$

6.3.3 Current

Compared with the wind fields, the current fields in the deep ocean have much larger time and space scales, and so fewer additional effects need be considered. The only additional event that needs to be considered that is not included in the hindcast data is the passage of an ocean front, for which a reasonable model is given in Section 6.3.5.

The major ocean currents in the open ocean have very little variation over the length of a MOB, so the values from the global hindcast can be applied over the length of the MOB. Also, the rate of change of global currents is small compared with the periods of the MOB and the time interval used for the data (3 days) should be sufficient to capture the changes in current speed and direction adequately.

Also, in the deep ocean, there is negligible variation of current speeds in the upper 100 ft of the ocean, within which the MOB lies, so there is no need for any adjustments of the current with depth below the surface.

Turbulence in the ocean, represented by ocean eddies, has time scale far greater than 3 days, and currents within these eddies vary with scales of the order of 100 km, so the variation within the length of the MOB can be neglected. The NRL current model is able to resolve these eddies, so these effects, if existing, should be present in the data.

Local wind-driven currents may have periods comparable to the inertial period at that latitude, equal to 0.5/sin(latitude). These are not included in the global current hindcast with a time interval of 3 days, but are modeled adequately by the local wind-driven current hindcast with a period of 1 hour.

As discussed in Section 6.4.3, there appears to be significant low bias in the modeled currents, so it is recommended that the modeled currents be increased significantly before being used in design situations.

6.3.4 Solitary Waves

An equation describing the specific balance between non-linearity and dispersion that enables soliton solutions was first expressed and solved by Korteweg and de Vris in 1895. Their solution is applicable to internal waves, which, for a two-layer fluid, have horizontal scale long compared to the depth of either of the layers. The "K-dV" equation is (Djordjevic and Redekopp (1978)):

$$\frac{\partial h}{\partial t} + c\frac{\partial h}{\partial x} + ah\frac{\partial h}{\partial x} + b\frac{\partial^3 h}{\partial x^3} = 0 \qquad (6.3\text{-}13)$$

where $\eta(x, t)$ is the deviation of the layer interface from the unperturbed level and the "environmental parameters" are:

$$c = \left[\frac{g(\rho_2 - \rho_1)h_2 h_1}{\rho_2 h_1 + \rho_1 h_2} \right]^{1/2} \tag{6.3-14}$$

$$a = \frac{3}{2} \frac{c}{h_1 h_2} \frac{\rho_2 h_2^2 - \rho_1 h_1^2}{\rho_2 h_1 + \rho_1 h_2} \tag{6.3-15}$$

$$b = \frac{c h_1 h_2}{6} \frac{\rho_1 h_1 - \rho_2 h_2}{\rho_2 h_1 - \rho_1 h_2} \tag{6.3-16}$$

The quantity c is the linear phase speed, a is the coefficient of non-linearity, and b is a measure of dispersion. Here, ρ_1 and ρ_2 are the densities of the upper and the lower layers respectively, h_1 and h_2 are their thicknesses, and h is the sum of h_1 and h_2.

For finite amplitude waves, the "K-dV" equation has the solution

$$h = h_o \sec h^2 \left[\frac{x - vt}{\Delta} \right], \quad h \quad \textit{positive} \quad \textit{downwards} \tag{6.3-17}$$

The K-dV solution has the interesting property that the soliton crest is downward if the upper layer is thinner than the lower ($a < 0$, $h_o < 0$), and upward if the reverse condition holds. In contrast to linear waves, the propagation velocity (v) and half width (D) are related to the amplitude of the soliton:

$$v = c + \frac{a h_o}{3} \tag{6.3-18}$$

$$\Delta = \left[\frac{12 b}{a h_o} \right]^{\frac{1}{2}}. \tag{6.3-19}$$

As soliton amplitude grows, the propagation speed increases beyond the linear phase speed and the characteristic width decreases. Spatial gradients thus grow rapidly, due to increasing amplitude and decreasing scale: $\eta_o / \Delta \sim \eta_o^{\frac{3}{2}}$.

These classical solutions are of relevance to solitary wave propagation only in shallow waters. In the deep sea, the effective lower layer depth (from the level where the water density changes abruptly to the sea floor) is comparable to or greater than the typical horizontal length scale of a solitary wave.

Seventy-two years following K-dV, Benjamin (1967) and Davis and Acrivos (1967) found solitary wave solutions for the useful limit $h_1 << \Delta << h_2$. Here, the wave scale is much greater than the upper layer thickness, much less than the lower. In the limit $h_2 \to \infty$ solutions take the form:

$$h = h_o \frac{\Delta^2}{(x - vt)^2 + \Delta^2} \qquad (6.3\text{-}20)$$

Where:

$$v = c\left(1 + 3/8\, h_o / h_1\right) \qquad (6.3\text{-}21)$$

$$\Delta = 4/3\, h_1^2 / h_o \qquad (6.3\text{-}22)$$

and,

$$c = \left[\frac{(r_2 - r_1)}{r_1} g h_1\right]^{\frac{1}{2}} \qquad (6.3\text{-}23)$$

This solution has come to be known as the Benjamin-Ono or "algebraic" soliton. Observationally, the differences between this "algebraic" soliton and the K-dV soliton are slight. (Figure 6.3.4-1, Kuznetsov et al. (1984)). The increase in propagation speed with increasing amplitude, predicted by both equations, is in accord with limited deep sea observations (Figure 6.3.4-2).

In the upper layer, horizontal current is independent of depth. It is related to vertical displacement by

$$u(x - vt) = v\frac{h(x - vt)}{h_1 + h(x - vt)} \qquad (6.3\text{-}24)$$

Here h_1 is the depth of the undisturbed upper layer and $h_1 + h$ is the depth as the soliton crest passes. This expression is frequently approximated:

$$u = v\frac{h}{h_1} \equiv u_o \frac{\Delta^2}{\left((x - vt)^2 + \Delta^2\right)} \qquad (6.3\text{-}25)$$

$$\text{Where :} \quad u_o = (v/h_1)h_o \qquad (6.3\text{-}26)$$

Note that it is not necessary to track the vertical displacement specifically at the interface. Near the sea surface, the magnitude of the vertical displacement, $h(z)$, increases approximately linearly with depth z, so that the ratio $h(z)/z+h_0/h_1$ (the vertical strain) can be measured at any convenient depth.

At issue is the appropriate value for the maximum current u_o. Precise measurements of horizontal velocity are difficult to obtain. Bole et al. (1994) reports that maximum currents of .50 to 1.50 m s^{-1} are "common" in the South China Sea. A 150-cm s^{-1} peak velocity was also mentioned by Osborne and Burch (1980), although, the accuracy of this estimate is unknown. Current speeds cannot exceed the phase speed of the disturbance (2.5 to 3.5 m s^{-1} in the deep sea).

For engineering design, we can consider a worst case wave of u_O =1.50 m s^{-1} in waters of h = 2.5 km depth. Assuming a typical buoyancy frequency profile,

$$c = 2.5 \text{ m s}^{-1}$$

$$h_o/h_1 = .6 \qquad (6.3\text{-}27)$$

$$v = 1.225\, c = 3.06 \text{ m s}^{-1}$$

$$D = 556 \text{ m}$$

The wave solutions for this case for u and for the vertical displacement of a surface whose undisturbed depth is 100 m are presented in Figure 6.3.4-3. Horizontal velocity can be regarded as depth independent in the top 30 m. Vertical displacement grows linearly with increasing depth, starting from zero at the sea surface.

The most troublesome aspect of the classical soliton solutions is the tendency for the length of the soliton to decrease with increasing amplitude. This results in surface strain rates $\partial u/\partial x$ which exceed 2×10^{-3} for the test wave (Figure 6.3.4-4).

In contemporary studies, equations more general than the Benjamin-Ono have been solved numerically (e.g., Lamb (1997)). Lamb's results are particularly germane to the MOB problem. He finds that, as solitons grow beyond a critical amplitude, they no longer tend to decrease in horizontal scale. In fact, the trend reverses and they grow in width (Figure 6.3.4-5). This has the effect of setting an upper bound on the strain rate and hence the tendency for the MOB to deform. However the lateral displacement of surface waters increases significantly (Figure 6.3.4-6).

Data to reconfirm Lamb's prediction have yet to be obtained. Thus, the more conservative algebraic solution is used for the design wave.

6.3.5 Ocean Fronts

The literature of fronts and frontal dynamics is extensive. The relevant aspect with regard to MOB is the lateral strain rate, $\frac{\partial u}{\partial y}, \frac{\partial v}{\partial x}$ of the upper ocean, where *u* and *v* are the *x* and *y* components of the water particle velocity. This will tend to rotate the MOB at the rate $\zeta/2$, where $z = \frac{\partial u}{\partial y} - \frac{\partial v}{\partial x}$ is the vertical component of fluid vorticity. The force required to resist this rotation depends on MOB orientation, being least when the MOB is aligned with the front, greatest when normal to the front.

Considering only open-ocean fronts, an arbitrary current profile of the form

$$u(y) = u_o \tanh (y/\Delta) \qquad (6.3\text{-}28)$$

can serve as a basis for engineering studies, where u_o is the maximum value of the current, and Δ defines the spatial scale. We select $u_o = .5$ m s^{-1} and $\Delta = 5000$ m as representative of a strong small-scale front. Modeled currents are independent of z and x.

At the front, the modeled vorticity is sufficient to rotate the MOB at 5×10^{-4} rad/sec or one revolution in 35 hours. In coastal waters vorticities ten times greater are possible.

6.4 Uncertainty in Data

The ultimate use of these environmental data will be in a reliability analysis of the MOB structural system. One input to this analysis is the accuracy of the data used. For this reason estimates have been made of the accuracy of the data included in this Specification. In some cases, such estimates are not based on quantitative data, and are the best estimates of the expert consultants that contributed to this work.

6.4.1 Wind

Uncertainties pertaining to wind speeds used in design are of two types:

1. Uncertainties pertaining to models used in conjunction with climatological data to estimate wind speeds.
2. Uncertainties pertaining to measured data

For the global data, the measurements going into the climatology used are generally reasonably accurate, and the uncertainties relate to how these data were processed and absorbed in the climatology. These issues are discussed in Section 6.4.1.1.

For the typhoon data, since there are relatively few measurements for a given typhoon, the issue is one of how to build a reasonable wind field from these few measurements. This is discussed in Section 6.4.1.2.

6.4.1.1 Global Winds

Data sets used in global hindcast efforts are limited by the use of data recorded at 6-hr intervals, which may result in relevant peaks being missed. Corrections for the consequent wind speed estimation errors can be developed on the basis of appropriate data.

The report from Oceanweather that accompanied the hindcast data in Appendix A explores the accuracy of the wind climatology used to drive the global wave hindcast, by examining the accuracy of the hindcast waves. The following summarizes the relevant parts of that report.

Cox, Cardone and Swail (1998), included in Appendix A assert that "recent studies with advanced third generation (3-G) ocean wave prediction models (Cardone et al. (1995)) show that, when such models are driven by accurate surface wind fields, nearly perfect simulations of the principal scale and shape (significant wave height and spectral peak period) properties of the surface gravity wave field result." From this assumption, a comparison was made of hindcast wave data with measurements from a number of buoys and satellite altimeters to estimate the accuracy of the wind data that drives the hindcast.

Figure 4 from the Oceanweather report, reproduced here as Figure 6.4.1.1-1 compares hindcast significant wave heights with satellite data in the North Atlantic. It shows that for a typical winter month, with significant height ranging from 0 to about 7 m, a negative bias in the hindcasts builds up to about 0.5 m (-7%), with a standard deviation increasing to about 1 m (14%). Above 7 m, the negative bias increases to about 2 m at 10-m significant height, (-20%) with the standard deviation remaining at about 1 m (10%).

Oceanweather's Table 3 shows a comparison of hindcast waves against all available buoys in the North Atlantic for one winter month. Overall, the mean error in significant wave height is about –0.16m (5%); the standard deviation of the difference between hindcast and measured heights is 0.82 m, yielding a scatter index of 27%; and the mean difference in peak spectral periods is –0.34 sec. (The scatter index is the standard deviation of difference between hindcast and measured values/mean of the measured values, expressed as a percentage.)

From these assessments of wave hindcast accuracy, we can return to the wind fields that drive them. Since the wave heights vary approximately as the square of the wind speeds, we can estimate that the global winds have a mean error of about -3%, and a standard deviation error or scatter index of about 10% to 15%. This estimate of the mean error is probably a fairly good one, but the scatter index only reflects those parts of the winds that drive the wave hindcast. Variations in wind speeds with periods that are less than about 12 hours will not affect the hindcasts and so are not included in this error estimate.

An alternative assessment on the accuracy of the winds in the NCEP/NCAR climatology has been provided by Dr. Robert Weller, using measurements from ocean experiments in which he has been involved. Appendix F describes these comparisons. The following discusses the results of comparisons between measurements and climatologies:

The measurement of surface wind from buoys moored in the open ocean provides the means to comment on the uncertainty in winds taken from climatologies such as the NCEP/NCAR climatology which provided the winds in this project. The Upper Ocean Processes Group (UOP) at the Woods Hole Oceanographic Institution (WHOI) deployed surface moorings at select locations around the world, measuring, among other items, wind speed and direction. The records run from several months to two years, and were taken every 15 minutes, then averaged over 1 hour. The anemometers on these buoys were typically 3 to 3.5 m above sea surface. For further details see Appendix F.

The accuracy of the buoy winds themselves is considered to be 3-6% based on laboratory calibrations and field intercomparisons (Weller et al. (1990); Weller and Anderson (1996)). The uncertainty comes primarily from the sensor response characteristics and buoy motion. There is little evidence of flow distortion problems associated with these research buoys.

Of particular concern when using model and/or climatological products is the loss of high frequency and high wavenumber information in the wind field as a result of the space/time averaging used in preparing these products. Figures 6.4.1.1-2 through 6.4.1.1-9 provide blow-ups of selected periods from the eight surface mooring records discussed earlier to illustrate the variability not resolved by models and climatology.

Figure 6.4.1.1-2 shows the wind associated with an intense, small low-pressure system in the Arabian Sea. This system was not forecast at the time and caught RV Thomas Thompson by surprise during a mooring recovery operation. This system was also not found in retrospective analysis of numerical weather prediction (NWP) model wind fields. Weller et al. (1998) discuss further problems with the NWP model fields in the Arabian Sea. They found that during the Southwest Monsoon NWP winds at the mooring site

could range from 5 m s^{-1} low to 8 m s^{-1} high compared to the buoy winds. These large differences were short-lived (hours to several days); however, it was also found that the NCEP and FNMOC (Fleet Numerical Meteorological and Oceanographic Center) mean wind speeds for the Southwest Monsoon were too low by 1.2 and 1.6 m s^{-1}, respectively, out of a mean of 11.2 m s^{-1}. Of the NWP models, that from ECMWF was the best; it gave a mean wind speed in the Southwest Monsoon at the buoy site of 11.3 m s^{-1}.

Comparison of the Arabian Sea buoy winds with contemporaneous winds from scatterometers on satellites found somewhat better agreement (Halpern et al. (1998)), with the best scatterometer product having a mean difference of less than 0.1 m/s. Although the algorithms for processing the satellite data are still in development (and other algorithms in this study gave mean differences of 0.5 and 0.6 m s^{-1}), this agreement improves over that found between the buoy and some models. Further, satellite winds have provided high spatial resolution (down to 4 km).

The NWP models perform better and the uncertainties in their surface winds is reduced in regions of the oceans that are more heavily traveled by commercial shipping. In these regions, more *in-situ* surface meteorological observations are available and used in initializing the NWP models. Moyer and Weller (1997) found that the mean differences in the Subduction experiment in the eastern North Atlantic between the surface mooring winds and the NCEP and ECMWF winds were between 0.16 m s^{-1} and 0.77 m s^{-1} across the five mooring array. Looking at the correlation between times series extracted from NCEP and ECMWF at the moorings, they found correlation coefficients of between 0.71 and 0.83. The agreement between the buoys' winds and the model winds is limited by the models' inability to replicate meteorological variability with short space and time scales. Figures 6.4.1.1-3 and 6.4.1.1-4 show 100-day long subsets of the Subduction North and Central buoy winds. Note, particularly at the North buoy, rapid but short-lived increases in wind speed sometimes accompanied by shifts in wind direction. These are related to the passage of atmospheric fronts. It is this high frequency variability that is not well replicated by the models and which leads to the degradation of the correlation between buoy and model time series.

In the Frontal Air-Sea Interaction Experiment (FASINEX), a particular effort was made to look at variability in the wind field on 15- to 50-km scales by setting a triangular array of 5 surface moorings with spatial separations between 15 and 50 km (Weller (1991); Weller et al. (1995)). Little spatial variability was found among the five FASINEX moorings. That which was observed was associated with small-scale synoptic systems whose low-pressure center tracked close to or through the array or with periods of low winds. Figure 6.4.1.1-8 shows ~70 days of data from one of the FASINEX moorings. While a number of short-lived events are evident in wind speed, the array showed that most such features were seen by the moorings as coincident, uniform changes in speed and directions. Figure 6.4.1.1-10 reproduces Figure 7 of Weller et al. (1995) to provide examples of the spatial variability. Comparison of the array winds with winds from ECMWF and FNOC (Fleet Numerical Oceanography Center, later FNMOC) showed basically good agreement, though ECMWF appeared to put too much energy into short

wavelength features and produced short-lived spikes in wind speed that were elevated relative to those seen at the buoys.

The NWP models use 6-hourly time steps and are run on spatial grids of typically 1 degree and larger. They are thus unable to replicate high frequency variability. This may become a significant source of uncertainty when the winds do have high frequency variability, as in tropical convective systems. The blow-ups of sections of the PACS N (Figure 6.4.1.1-5) and TOGA COARE (Figure 6.4.1.1-9) do show such short-lived spikes in wind speed. PACS is still in the water, but the wind data from COARE has been extensively compared to model products (Weller and Anderson (1996)). Figure 6.4.1.1-9 reproduces an overplot of COARE buoy and ECMWF NWP data. Note the inability of the model to track the observed high frequency variability in wind speed. A consequence of the model's difficulty with high frequency events is that it also yields means speeds with larger error during periods characterized by squalls. Table 6.4.1.1-1 compares the model winds with the buoy during periods of large-scale atmospheric convection (westerly wind bursts), during low winds, and during a period characterized by squalls.

		Westerly wind burst		Low wind		Squalls	
	units	Buoy	ECMWF	Buoy	ECMWF	Buoy	ECMWF
Speed	$m\ s^{-1}$	7.38	6.32	2.19	2.33	6.17	5.13
Direction	°	128.0	108.1	248.0	353.2	126.1	109.3

Table 6.4.1.1-1 Comparison of Mean Wind Speeds and Directions from the TOGA COARE buoy and the Nearest Grid Point of the ECMWF NWP model for different climatological conditions in the western tropical Pacific.

In general, then, the buoy data indicate the need for some caution when using NWP model winds. They have been found to both underestimate and overestimate the observed winds. Their mean values may be incorrect by ~1 $m\ s^{-1}$ and instantaneous values from the models may be incorrect by up to 5 to 10 $m\ s^{-1}$. While the mean wind patterns and synoptic weather patterns with scales of ~100 km and larger (thus matching the roughly 1° gridding of the models) are resolved, sharp atmospheric fronts and small convective systems are not resolved. Thus, some provision should be made in the design studies for the MOB of considering the possibility of rapid wind events not captured in the NWP model winds.

The NCEP/NCAR wind data were selected to be the primary wind data since it was recorded at the same time that wave hindcast data was found, and is available for the length of time of the wave hindcast, thus allowing joint statistics between wind, wave and current to be developed, an ability that had been considered from the start of the project to be important. The wind data allows computations of MOB responses that do not vary much over time periods less than about a day, but clearly cannot be used, unmodified, as a wind source for effects that vary over time segments less than this, due to the lack of detail over these time periods.

Thus the data could be used, for instance, to determine fuel and thruster requirements to keep the MOB on site, provided the dynamic positioning system (DP) is not set up to respond to every wind gust that attempts to move it off site, but is only required to keep it on site in an average sense over time periods of a day or so. If it considered important to have the thrusters keep it more accurately on site over periods of the order of an hour or so, this wind data clearly does not have enough high frequency information for this purpose.

Another situation where the high-frequency detail in this wind data might be inadequate is the prediction of operational availability for aircraft operations. If landing is possible in a certain wind speed, even if the mean 6-hourly wind is above that speed, there may be windows of time long enough to land aircraft. As a result the use of the unmodified data for an operational availability study may result in a lower number of hours annually available for landing than would be found if wind with more high-frequency data was used.

In the same way, items affected by peak wind gusts will have the wind speeds underestimated by winds averaged over 6 hours.

Estimates of wind spectra have been given in Section 6.3.1.3 due to effects of turbulence there is some question about using this spectrum up to periods of several hours, to fill in the data for times less than the 6 hourly intervals at which the data is provided. To improve this wind data, it would be desirable to spend more time to investigate the variation of wind speeds over periods of the order of a few hours, and see how they related to the 6-hour mean values, and the recommended spectrum. This could be carried out by locating relatively short lengths of wind data at sites near the four deployment sites, developing measured wind spectra over the periods of interest, and comparing to the spectrum defined in Section 6.3.1.3, for a range of wind conditions.

6.4.1.2 Typhoon Winds

Major uncertainties are attached to the maximum wind speeds near the surface in tropical cyclones of hurricane or typhoon strength. To date, not a single reliable physical measurement of such speeds exists. Calibrations of models used in simulations of the maximum wind speeds are therefore performed against relatively weak winds measured far from the center. As for surface wind speeds near the storm's eye, the simulations provide results that must be compared with beliefs - subjective estimates - as to what those speeds may be expected to be. Though such subjective estimates can be useful, no definitive scientific validation of simulation results for very strong tropical cyclone speeds exists to date.

Simulations used for hindcasting are currently based on models wherein the equation of motion of the atmospheric vortex flow is averaged over the height of the planetary boundary layer. According to Shapiro (1983), such models, referred to as a simple slab models, "cannot describe the detailed structure of the boundary layer, especially near the eye wall." Nevertheless, with state-of-the -art enhancements such as those described by

Thompson and Cardone (1996), they are capable of yielding reasonable estimates. For the maximum wind speeds near the tropical cyclone center the physical modeling errors are estimated subjectively to be of the order of 15%, perhaps even 20%.

One important feature of extreme winds in hurricane-prone regions is that their variability is considerably higher than the variability of winds in non-hurricane regions. For this reason, for any given risk level, in hurricane-prone regions wind load factors (i.e., partial factors reflecting the uncertainty with respect to the wind loading) must be significantly higher than their counterparts in non-hurricane regions (Simiu and Heckert (1998)). This feature was not known to the writers of the ASCE 7-95 (1995) Standard and its predecessors, but is now reflected in the draft ASCE 7-98 (1998) Standard.

The lack of detailed wind measurements during large typhoons make estimates of the accuracy of the wind fields difficult. Due its proximity to the U.S. hurricanes, the Gulf of Mexico has been followed more closely than those in the Northwest Pacific. As a result, the accuracy of the hindcasting of hurricanes in the Gulf of Mexico is rather better than in the Northwest Pacific especially for those that occurred decades ago when there were not the same facilities for following and measuring typhoons.

Some of the uncertainty in a hindcast comes from the uncertainty in the track, and with aircraft, satellite and shore-based radar, the eye can be estimated to within about 10 km. Although the uncertainty in the Northwest Pacific typhoons is certainly considerably higher, this particular issue can be essentially eliminated for design purposes by processing the hindcast data in such a way as to allow random variations in the storm track when developing statistical information. This process has been incorporated in the statistical software MOBENV developed during this project.

Validation studies of hindcasts in the Gulf of Mexico during hurricane Andrew were conducted using wind measurements that were never closer than 50 km from the eye. From these, it has been estimated (Cardone, 1996 Hurricane Andrew, Effects on Offshore Platforms, Phase II, Joint Industry Project, January 1996) that the winds hindcast in the major 1992 hurricane Andrew have a scatter, taking into account the uncertainty in the track, of $^{+}$/- 2.5 m/s in speed and $^{+}$/- 25° in direction, r.m.s. values, and systematic errors are probably less than half of these values. The peak winds developed by Andrew were estimated to be 48 m/s, while those in the supertyphoon Kit were 60 m/s.

The estimated accuracy of the winds in Northwest Pacific typhoon hindcasts is presumably somewhat less than this.

Probabilistic modeling is an additional source of errors. Tropical cyclone speeds have in the past been modeled by the Weibull distribution, which is an Extreme Value distribution of the smallest values. In fact, extreme value distributions of the largest values can be only of the Fretchet type, of the Gumbel type, or of the reverse Weibull type. As was indicated in Section 5.2.1.4, according to statistical studies conducted for the Gulf of Mexico and U.S. Atlantic coast, hurricane wind speeds considered without regard for direction are described probabilistically by the reverse Weibull distribution. For large mean recurrence intervals, as may be of interest for ultimate capacity calculations, estimated wind speeds are very sensitive to the type of distribution being assumed. For example, for a coefficient

of variation of the population of extreme wind speeds of 0.2, the ratio of the 10,000-year wind speed to the 50-year wind speed is 1.52 if the variate is described by a Gumbel distribution, and 1.2 if it is described by a reverse Weibull distribution with tail length parameter c= - 0.2.

Finally, the extreme wind speed estimates are affected by sampling errors due to the relative small size of the statistical data sample (say, 20 to 100 years) on which the estimates are based. For hurricanes, the standard deviation of the sampling errors was estimated to be about 10% for 50-year wind speeds based on a climatological data sample of about 100 years (Batts, Cordes and Simiu (1980)). If the sample is only about 20 years, the estimated standard deviation of the sampling errors is about $(5/2)^{1/2}$ x 10% = 15%. The sampling errors are an increasing function of mean recurrence interval. For example, for a 10,000-year mean recurrence interval, the estimated standard deviation of the sampling error for estimates based on about 100 years of hurricane data is about 25%; for a sample based on 20 years of data it is about 40%. Such errors may be reduced to some extent by spatial smoothing (Casson and Coles (1998)).

It is emphasized again that, for loads that would cause structural failure and would therefore be required to have very long mean recurrence intervals, the uncertainties in the estimation can be very large. The uncertainties are even more severe if they involve joint probability distributions of wind, wave and current distributions.

6.4.1.3 Accuracy Associated with Other Wind-related Issues

Vertical Variation of Wind Speed

For relatively low wind speeds, the flow stratification is, in general, not neutral. Neutral stratification is the condition prevailing in the atmosphere when the vertical motion of an air parcel is sufficiently rapid that the heat exchange of that parcel with its environment may be considered to be negligible. In such flow, temperature effects can be significant, and the mean speed profile can deviate significantly from the logarithmic law -- see Simiu and Scanlan (1996), pp. 49-51. According to estimates in Simiu and Scanlan (1996), the deviations from the logarithmic law tend to be significant (i.e., about -15% at 15 m elevation) for U(10) ≈ 5 m/sec, but decrease fairly rapidly for larger speeds.

For moderate wind speeds (say, 10 m/s at 10 m above the ocean surface) the use of the logarithmic law entails errors of the order of 5% or less (see Simiu and Scanlan (1996), p. 50).

Wind Speed Spectra

Errors in the estimation of the spectra in equations 6.3-2 and 6.3-3 are much larger for very low frequencies. It is tentatively suggested that for frequencies f (Hz) such that fz/U(z)>0.1, the errors in the estimation of the spectral ordinates may be as high as roughly 50%. (U(z) is the wind speed at elevation z). For frequencies fz/U(z)<0.1, the

errors are likely to be significantly higher – perhaps up to +100%, -50%. (+40%,-30% on velocity.)

Error estimates for cross spectra are somewhat higher, possibly 1.5 times or even twice as high as those indicated for spectra for both higher and lower frequency ranges. An alternative estimate of uncertainties is inherent in the spread in the values of relevant parameters in Figures 5.2.1.3-9 and 5.2.1.3-10.

6.4.2 Waves

It is generally recognized that good wave hindcast models reproduce wave fields with an accuracy that depends on the accuracy of the winds used to drive the models. The model errors are not well known because it is difficult to determine the distribution of error sources between the models themselves and the winds used to drive them. Given the sensitivity of the models to the driving winds the model accuracy may be well described in terms of the wind accuracy. The global hindcasts are dominated by fully developed waves and these are the largest waves for a given wind field. The significant heights and peak periods at full development (equations 5 and 6 of Appendix H) are proportional to the wind speed to the power 2 and 1 respectively, so that a percentage error in the wind speed, ε, will cause percentage errors in the significant height and peak period of 2ε and ε respectively. The typhoon hindcasts, on the other hand, are very sensitive to the degree of development, which is dependent on size and strength of storm and, most importantly, on the pattern of progression of the storm center with respect to the target site. (As described in Appendix H, the procedure for dealing with such data should involve more than a straight hindcast of historical storms. Instead, the sensitivity to storm track and progression at rates near the group velocity of the longest waves should be explored.)

6.4.2.1 Global Hindcast

The report from Oceanweather that accompanied the global hindcast data in Appendix A explores the accuracy of the global wave hindcasts. The following summarizes its findings:

The preliminary evaluations of hindcast made with NRA wind fields (as used in the Oceanweather hindcasts for the project) suggest that at least in extra-tropical areas the mean error in significant wave height overall is less than 0.5 m (low bias) and the scatter index (standard deviation of difference between hindcast and measured values/mean measured values, expressed as a percentage) is about 25%. The mean error in T_P (spectral peak period) is less than 0.5 sec, and the scatter index is about 35%.

6.4.2.2 Typhoon Hindcasts

Estimates of the accuracy of winds used in wave hindcasts in large Gulf of Mexico hurricanes were given in Section 6.4.1.2. Accuracy of waves could be based on the wave

heights varying as the wind speed squared although this is based on fully developed seas which is certainly not the case in typhoons. Nevertheless, on this basis, an estimate of wave hindcast accuracy could be made from estimates of the wind accuracy given in that section.

Studies reported by Cardone (1996) compared wave measurements during the passage of Hurricane Andrew with hindcast values. As for winds, no measurements were within 50 km of the storm center. At all deepwater sites, the maximum hindcast significant heights H_s were within 1 m of the measured maximum values. The largest deepwater waves were measured at Bullwinkle platform, which was never closer than 74 km from the storm center. The peak hindcast H_s was 8.7 m, while the measured value was 7.9 m. Once again, the issue of the sensitivity of results to track location, mentioned in Section 6.4.1.2 should be considered, but, again, for design purposes this can be eliminated by using randomized tracks for the typhoons.

In Figure 3 in the typhoon hindcast report in Appendix B, Oceanweather compares hindcast with measured wave data. The report then estimates the accuracy of their typhoon wave hindcast as having at the peak value a mean error of less than 20 cm, and rms error of less than 1 m.

6.4.3 Currents

Our recommendation is to adjust the model currents and add to them time series of the local tides and wind-driven flow. By comparison with observed upper ocean time series, we believe this to be an approach that minimizes the uncertainties in the hindcasts of currents. The correction for each is discussed below in turn:

Winds can excite the resonant response of the upper ocean as discussed before. The closer the characteristics of the wind are to the near-inertial response, the stronger the resulting currents. For example, at 30° N, if the wind direction turns clockwise with time, taking 24 hours to come around and thus matching the local inertial frequency, strong surface currents will be generated. More generally, the winds also drive lower frequency currents. These currents are essentially linearly superimposed on other background flows in the ocean, so our procedure is to use realistic wind and mixed layer depth time series to predict the local wind-driven currents, including the potentially strong near–inertial currents.

The hindcast of the sub-inertial frequency wind-driven currents has been found in general to be fairly accurate, approaching 20% if the winds and mixed layer depth are themselves accurate to about 5%. In general, the hindcast of near-inertial currents has been similarly successful. However, it is necessary to caution that near the resonant frequency, response amplitudes can be quite large, with 1 m s^{-1} surface currents observed; that the physics of the processes that damped near-inertial currents are not well-understood and only crudely included in the model; that changes in mixed layer depth can dramatically change the response amplitude and can themselves come about in response to the wind (wind-driven deepening due to mixing or shoaling/deepening due to divergent /convergent surface

flow); and that the relative vorticity of the background flow field can alter the local inertial frequency, making it difficult to achieve accuracy in hindcasting the near-inertial currents. Thus, it is appropriate in general to assign a larger uncertainty to the near-inertial currents, say 30%, and to keep in mind the contingency that various environmental factors could coincide to produce a pulse (several local inertial periods in duration) of strong inertial currents localized to the mixed layer. To simulate this contingency, the hindcast near-inertial currents, at their peak, should be considered to be potentially too low by 50%.

The surface wind fields, as discussed earlier, generally have large spatial scales (100s of km). Spatial variability in the wind-driven currents will be introduced by the wind and mixed layer depth. Where the wind scales are large, the wind is not a source of spatial variability. Wind scales may be small in the open ocean, as discussed earlier, in small intense systems and at sharp features such as squall lines. However, roughly one inertial period is required for the momentum from the wind to accelerate wind-driven currents and such small scale but transient winds do not introduce spatial structure of concern.

Because the momentum from the wind is distributed over the mixed layer depth, spatial change in mixed layer depth will lead to spatial differences in the wind-driven response. Again, the spatial scales of the mixed layer depth field are generally large (10s to 100s of km). However, an ocean front or eddy could have a change in mixed layer depth over 10 km and less. Thus, in special locations, such as fronts and eddies, one should anticipate change in wind-driven flow proportional to the change in mixed layer depth.

The background flow field that is associated with the large-scale geostrophic circulation is provided by the global model, and the first comparisons presented here are between the global model data and measurements. Figures 6.4.3-1 and 6.4.3-2 compare maximum and mean currents at the sites of the instrumented buoys discussed in Appendix F, with those predicted by the global hindcast, as a function of site number. The same data are replotted in Figures 6.4.3-3 and 6.4.3-4 as a function of latitude. This makes the regional character of model performance more evident. Within 5° of the equator, the model currents are too strong, and it is recommended that they be reduced by 20%. In subtropical regions up to about 30°N, the model currents are too weak. The difference is greatest where the ocean is known to have frontal and/or eddy activity, such as in the FASINEX and Arabian Sea regions. It is suggested, in general, that the model currents be increased by 30% and that at ocean fronts and in areas of eddy activity (as might be judged by satellite altimetry), that the model currents be increased by 100%. Measurements at the ASREX buoy are considered to be too short to have stable statistics. The MLML buoy, because of the presence of the subarctic front, shows a similar underestimation in the model as that seen at the FASINEX buoy. However, off eastern Canada, at the SESMOOR buoy, the model is too strong.

After comparing the predicted global currents to the measured currents, the local wind-driven currents were added to the global currents. For this operation it was necessary to have both sets of data and the measured data with the same time step. This was accomplished by interpolating the global currents (that were recorded at 3 day intervals) to be at 1 hour intervals. Since there were some dropouts of the measured data in winds

(used to compute the local wind-driven currents) and currents, the lengths of time used in these comparisons do not necessarily match those in the previous study of currents from the global model.

The results are shown in Figs. 6.4.3-5 through 6.4.3-11 for each of the seven sites studied. The upper plot on each page shows the global currents, the next the local wind-driven currents, and the third is the sum of these two. The bottom plot shows the measured current. An examination of these plots shows that although the mean and maximum currents predicted by the sum of the two components generally gives a reasonable estimate of the maximum and minimum, there is essentially no detailed correlation between the individual or total predicted current, and the measured current. This is shown even more forcefully in the scatter plots of Fig. 6.4.3.12. In these plots, at each time a point is placed on the plot with the abscissa as the predicted value using the sum of the global and local currents, and the ordinate as the measured current. To interpret this data, refer to Fig 6.6.8.2-1 which shows, generally, the effect of various types of lack of equality of any two sets of data plotted. From Fig. 6.4.3.12 it can be seen that there is very little if any correlation between individual points, and there is a general bias to low predictions. However, as mentioned above, the mean and maximum values are generally not too unreasonable, with about 35% error overall.

Table 6.4-1 shows the results of these comparisons in a quantitative form.

Experiment	**Arabian Sea**	**Subduction (C)**	**FASINEX**	**Subduction (N)**	**ASREX**	**SESMOOR**	**MLML**		
Site Number	26	28	36	27	31b	35	32		
Latitude (N)	15.5	25.5	27.0	33.0	33.9	42.5	59.5		
Predicted Current									
Global									
Max.	0.533	0.198	0.085	0.207	0.246	0.664	0.238		
Mean	0.157	0.063	0.037	0.062	0.104	0.233	0.140		
Local Wind-driven									
Max.	0.736	0.593	0.191	0.268	0.154	0.256	0.271		
Mean	0.093	0.072	0.030	0.042	0.039	0.067	0.058		
Total Predicted									
Max.	0.701	0.530	0.223	0.319	0.304	0.756	0.357		
Mean	0.187	0.097	0.050	0.079	0.113	0.246	0.152		
Measured Current									
Max.	1.273	0.373	0.877	0.704	0.495	0.909	0.712		
Mean	0.258	0.091	0.243	0.153	0.269	0.243	0.211		
Ratio of Predicted Global to Measured Current								**Mean**	**Std. Dvn.**
Max.	0.4	0.5	0.1	0.3	0.5	0.7	0.3	0.41	0.19
Mean	0.6	0.7	0.2	0.4	0.4	1.0	0.7	0.55	
Ratio of Predicted Local Wind-driven to Measured Current								**Mean**	**Std. Dvn.**
Max.	0.6	1.6	0.2	0.4	0.3	0.3	0.4	0.53	0.44
Mean	0.4	0.8	0.1	0.3	0.1	0.3	0.3	0.32	0.21
Ratio of Total Predicted to Measured Current								**Mean**	**Std. Dvn.**
Max.	0.55	1.42	0.25	0.45	0.61	0.83	0.50	0.66	0.35
Mean	0.72	1.06	0.21	0.52	0.42	1.01	0.72	0.67	0.29

Table 6.4-1 Comparison on Predicted and Measured Currents at Experimental Buoys

The top 3 sets of (2-row) data show, for each of the experiments, the maximum and mean values of (1) the global model currents, (2) the local wind-driven currents covering the same period, and (3) the maximum of the total of the two. This is followed by the same statistics for the measured current covering the same period. To give a quick comparison of the two models and the sum with the measurements, the 3 lower sets of rows give the above predicted maxima and means divided by the measured maxima and means. Finally on the right hand side of the table the mean and standard deviation of the last ratios are shown over all the experiments included.

Looking primarily at the accuracy of adding the time series formed by adding the global and local, we see from the last two rows near the bottom that the total modeled current gives mean values and maximum values about $^2/_3$ of the measurements. The scatter is high however, with a standard deviation of about ½ of the mean value.

In general, with the limited comparison possible, it appears that the models major currents, such as the zonal equatorial current and western boundary currents, may be too strong and that flows in the interior of the ocean are too weak. However, the limitation in this conclusion is that only a handful of sites were available for checking the performance of the model. This, in itself, indicates that there are areas of the ocean in which the realism of the model has not been assessed and that an additional uncertainty must be attached to use of the model at locations away from the comparison sites.

6.4.4 Internal Waves

Due to the limited amount of data on internal waves that is available, it is not possible to make any generalizations on the accuracy of the information given in Section 6.2.4. The recommendations provided there are the best estimates from Robert Pinkel, an expert in the field, from measurements where these waves have been observed. It is not possible to say at this time at any site what the distributions of different characteristics that describe internal waves are.

6.5 A Selection of Data at Deployment Sites

This section provides a look at the environmental data at the four deployment sites. The data are presented in a set of histograms giving the number of occurrences for a range of values for each variable. These plots were all created using the program MOBENV provided with this Delivery Order.

The first set are for the four deployment sites, using the global data, while the second set is for the typhoons at the Northwest Pacific site.

All significant wave heights are in meters and wind and current speeds are in m/sec.

6.5.1 Global Data at Deployment Sites

Figures 6.5.1-1 through 6.5.1-16 show the winds, waves and currents at the four deployment sites. For ease of analysis, these were all created using only the five years 1979 to 1983. Inclusion of the remaining years would not change the overall character of each of these distributions.

The global environmental data in Table 6.5.1-1 covers the full lengths of the hindcasts. For each variable, the maximum and the mean values are shown in the table. For waves, the maximum is likely to be of importance for survival, while the mean may reflect the severity of fatigue. For wind and current, the maximum value may govern the size of thrusters required to keep the MOB on station, while the mode affects the total fuel usage.

As has been pointed out previously, the three tropical sites, Northwest Pacific, Arabian Sea and Sea of Japan are subject to typhoons which generate the largest winds and waves, but are modeled poorly by the global hindcast. This is also the case for the local wind-driven currents, which are computed from the global winds. Therefore, the maximum values of wind, wave and local wind-driven currents associated with these three sites are shown in parenthesis, and should not be considered as reliable data. The global currents are driven by winds with larger space and time detail, and should be reasonably accurate even for these tropical sites.

At these three tropical sites the global modeling of non-typhoon conditions should be quite reliable, since the scale of these atmospheric effects are more in keeping with the global modeling. As a result, the mean values shown can be considered to be reasonable estimates of frequently-occurring conditions.

Site	**North Atlantic**	**Northwest Pacific**	**Arabian Sea**	**Sea of Japan**
Global Data:				
Significant Wave Height - Maximum	16.3	(8.9)	(5.7)	(7.2)
- Mean	3.8	2.0	1.5	1.3
Wind Speed – Maximum	32	(21)	(16)	(22)
- Mean	9.5	6.7	6.1	6.0
Global Current - Maximum	0.55	0.87	0.64	1.02
- Mean	0.11	0.14	0.13	0.21
Local Wind-driven Current – Maximum	0.47	(0.85)	(0.85)	(0.91)
- Mean	0.03	0.08	0.08	0.06
Total Current - Maximum	0.72			
- Mean	0.11			
Typhoon Data:				
Significant Wave Height - Maximum		18.817.5		
- Meanode		(3.92)		
Wind Speed – Maximum		510		
– Meanode		(13.68)		
Local Wind-driven Current – Maximum		2.278		
– Meanode		(0.1805)		

Table 6.5.1-1 Summary of Environmental Data at Deployment Sites

6.5.2 Typhoon Data at Northwest Pacific Site

Typhoon data at at the Northwest Pacific site are also shown in Table 6.5.1-1. The data is from taken from the 22 most intense typhoons in 50 years that passed through the 2° x 2° box around the site. The typhoon hindcasts are designed to model the smaller temporal and spatial conditions of a tropical storm, and so the data from these hindcasts should represent the most severe conditons at this site well. However no information is given by the typhoon hindcasts about day to day conditions, and so the modal values of wind, wave and current read from the plots have been set in parentheses to indicate that they are not reliable indicators of the general conditions at the site. The global analyses provide data for these conditions. The random path option (described in Section 6.6.5.4) was use for this analysis, with a 4 x 4 grid, which essentially considers all the typhoons as having 16 different random paths in the vicinity.

6.5.3 Comparison of the Four Deployment Sites

The data in Table 6.5.1-1 should be reviewed with the issues raised in Sections 6.5.1 and 6.5.2 in mind. It should also be noted that the data are not design data, but simply the data that were hindcast during the appropriate periods of time. For design purposes something like a 100-year return period seastate would be expected to be applicable, but since the MOB may be quite sensitive to the wave frequency and direction, the extreme wave conditions may not be those with the largest wave heights. The global data represents only 18 or 23 years of hindcasting, so we would expect the 100 year values to be somewhat larger than these. On the other hand, the typhoons at the Northwest Pacific site were specifically chosen to be the most intense during a 50-year period, so the peak wind, wave and current from those hindcasts are closer to design values. The opposite is true of the mean values. The global data used were for the full five years, so the modal values should represent typical conditions quite well. However, the typhoon data are only for the most intense typhoons, so, give no indication of typical conditions at the site.

With these observations in mind, we can compare the four sites.

The North Atlantic site has the highest background of large winds and waves, as seen by the highest mean values for both wind and waves. So it is likely to be the worst site for fatigue, and perhaps for operational availability considerations. Needless to say, this is to be verified in design given a specific concept/configuration of the MOB.

The largest significant wave at the North Atlantic in 23 years was 16.3 m. The 50 year return period value would be a little larger than this. The largest significant wave height in 50 years of typhoons at the Northwest Pacific was 18.8 m. It can be seen that the extreme sea states at these two sites are therefore probably quite similar, the more critical seastate possibly being determined by wave directionality or wave period distributions. Thus, it is fairly clear that both the North Atlantic and the Northwest Pacific should be candidates for the most severe winds and waves.

In passing, it is interesting to compare these values with 100 year design wave heights in the Gulf of Mexico and North Sea. The 18.8 m significant wave at the Northwest Pacific

site would result in an individual wave height of about 1.9 x 18.8 m = 36 m. (117 ft) Even without scaling this up for the 100 year return, this is much greater than the 100 year return value of about 22 m (70 ft) generally appropriate for hurricanes in the Gulf of Mexico, showing that the super-typhoons of the Northwest Pacific are much more severe than those of the Gulf of Mexico.

Similarly, based on the maximum significant wave height for 23 years of 16.3 m, the North Atlantic site would have a 100 year return period significant height of about 1.1 x16.3 m = 17.9 m, which would result in individual waves of about 1.9 x 17.9 m = 34 m (112 ft). This is somewhat larger than the typical 100-year return wave in the North Sea of 30 m (100 ft), due presumably to the more open conditions of the North Atlantic.

From the start of the project, it was known that the Northwest Pacific site has the most severe typhoon conditions, so there were no dedicated typhoon hindcasts run at the other two tropical sites. This site therefore can be used for the worst tropical site.

For currents, the Sea of Japan has the highest mean and maximum global and local wind-driven currents so that site probably has the highest general current activity. While the maximum global currents should be reasonably well predicted, the local wind-driven currents computed from the global winds suffer from poorly defined wind fields during typhoons at the three tropical sites, and so should not be considered reliable for predicting maxima. As for waves and winds, the wind-driven currents from typhoons should be used for maximum currents at the Northwest Pacific Site.

6.6 MOBENV – The Statistical Software

6.6.1 Overview and Objectives

The program MOBENV is a computer program to study the hindcast wind, wave and current data assembled for this project. It is designed to be used by users wishing to access and get a general idea of the environmental data that have been collected for the project and perform a variety of statistical combinations. However, it is not intended as a rigorous statistical analysis tool that will be used in the selection of the design metocean conditions.

The reason for this is that a MOB would be designed under the Classification Guide being written by the American Bureau of Shipping (ABS) which is reliability-based and will provide the theoretical background to develop the design and the associated environmental conditions. The actual metocean conditions and seastates for design will be structure-dependent and cannot be anticipated until the form of the MOB is known. Different seastates may control different concepts and/or concept components. Therefore, emphasis has been placed on making an easily-used software package for the user to explore the wind, wave and current data at any of the sites and produce statistical tables or plots of these data.

6.6.2 Program Basic Properties

The main program is written in MATLAB largely because of its graphics capabilities. To use the program the user must have access to this proprietary program, but, due to popularity, most potential users should have no trouble getting such access. The main program interacts with a Fortran program that reads the data off the source disks, because of its greater flexibility in reading of disk files.

The input to the program are the files from the various hindcasts described elsewhere in this report. These are also summarized in Section 6.6.3. The program then displays tables and plots on the screen, and saves them to an output file on the computer's disk.

6.6.3 The Environmental Data (Input)

The data from the environmental hindcasts consist of the following (for more details see Appendices A, B, C and D):

6.6.3.1 General Hindcast Data

General Hindcast Wind and Wave Data:

Hindcast wind and waves for 23 years at 25 sites (4 deployment and 21 transit sites) are from the Oceanweather hindcast.

The data reside on a CD-ROM created by Oceanweather. This CD-ROM has 1 zipped file for each site, named *GROW_gridno_74_96.zip*, where the actual grid point number is represented in the name by *gridno*. Each such zipped file contains 1 file for each year, named *yr0101_gridno.asc*, where the actual year is represented by the name *yr*. These files can be extracted with commonly available programs such as WinZip, available on the Web at http://www.winzip.com or PKZIP at / http://www.pkware.com/. Each yearly file is 0.38 Mbytes in size, so that 25 sites for 23 years would need about 220 Mb of disk space. It may, therefore, be desirable to only extract the data needed for a given session.

These data consist of the following time histories, recorded at 6-hour intervals:

WD	Wind Direction from which the wind blows, clockwise from true north, in degrees (meteorological convention)
WS	Wind Speed; 1-hour average of the effective neutral wind at 10m height, in m/sec
ETOT	Total Variance of Total Spectrum, in m^2
TP	Peak Spectral Period of Total Spectrum, in sec.
VMD	Vector Mean Direction of Total Spectrum to which waves are traveling, clockwise from true north, in degrees (oceanographic convention).

The following six variables are from dividing the directional wave spectrum into two components, a "sea" and a "swell":

ETOTSEA Total Variance of Primary Partition (sea), in m^2.

TPSEA Peak Spectral Period of Primary Partition (sea), in sec

VMDSEA Vector Mean Direction of Primary Partition (sea), same rules as VMD.

ETOTSW Total Variance of Secondary Partition (swell), in m^2.

TPSW Peak Spectral Period of Secondary Partition (swell), in sec.

VMDSW Vector Mean Direction of Secondary Partition (swell), same rules as VMD.

The following nine variables are from dividing the directional wave spectrum into three components, a "sea" and a two "swell" components:

ETOTTR1 Total Variance of First Partition (sea), in m^2

TPTR1 Peak Spectral Period of First Partition (sea), in sec

VMDTR1 Vector Mean Direction of First Partition (sea), same rules as VMD.

ETOTTR2 Total Variance of Second Partition (swell), in m^2.

TPTR2 Peak Spectral Period of Second Partition (swell), in sec

VMDTR2 Vector Mean Direction of Second Partition (swell), same rules as VMD

ETOTTR3 Total Variance of Third Partition (swell), in m^2.

TPTR3 Peak Spectral Period of Third Partition (swell), in sec.

VMDTR3 Vector Mean Direction of Third Partition (swell), same rules as VMD.

HS Significant Wave Height, in m.

M01 First Moment of Total Spectrum

M02 Second Moment of Total Spectrum

General Hindcast Global Current Data:

Hindcast global currents for 18 years at 25 sites (4 deployment and 21 transit sites) are from the Navy Research Laboratory hindcast (reorganized by BNI).

These data reside on a CD-ROM, created by BNI by reorganizing the original NRL files. This floppy disk has 1 zipped file called *nrl.mob.zip*. This file contains 1 file for each grid point for each year, named *nrl.gridno.year*, where *gridno* is the grid point number, and *year* is the actual year. These files can be extracted with commonly available programs such as WinZip. Each extracted file is 6.3 Kbytes in size, so that 25 sites for 18 years would need about 3 Mb of disk space to hold, which is not very large.

These data consist of the following time histories, recorded at 3-day intervals:

CD Current Direction to which the current flows, clockwise from true north, in degrees (oceanographic convention)

CS Current Speed in m/sec.

General Hindcast Local Wind-Driven Current Data:

Hindcast local wind-driven currents for 23 years at 25 sites (4 deployment and 21 transit sites) are from BNI. These are meant to supplement the currents from NRL.

These data reside on a CD-ROM, created by BNI. This disk has a zipped file called *global.wind.currents.zip*. This file contains 1 file for each grid point, named *globall.gridno*, where *gridno* is the grid point number. These files can be extracted with commonly available programs such as WinZip or PKZIP. Each extracted file is 2.4 Mbytes in size, so that 25 sites would need about 60 Mb of disk space to hold. It may therefore be desirable to only extract the data needed for a given session.

These data consist of the following time histories, recorded at 1-hour intervals:

CD Current Direction to which the current flows, clockwise from true north, in degrees (oceanographic convention)

CS Current Speed in m/sec.

6.6.3.2 Typhoon Data

Typhoon Hindcast Wind and Wave Data:

Hindcast wind and waves for 25 intense typhoons at the Northwest Pacific site are from Oceanweather.

These data reside on a CD-ROM created by Oceanweather. This CD-ROM has 6 zipped files covering all the archived grid points. These locations are referred to by the Oceanweather grid point number, only. Thus grid points 5263 through 5999 are on the file *Gpts005.zip*, and points 6000 through 6999 are on *Gpts006.zip*, etc. Each such zipped file contains one file for each grid point, named *gridno.asc*, where the grid point number is represented by *gridno*. All 25 typhoons are stored sequentially on each such unzipped file. Each unzipped file is 0.27 Mbytes in size, so that 2112 grid points archived would need about 570 Mb of disk space to hold. It may, therefore, be desirable to only extract the data needed. The only grid points that are needed by MOBENV are the 25 grid points listed below (shown as they occur in plan view of the region), so there is no need to extract more than these.

Northwest				Northeast
9001	9004	9005	9006	9009
8641	8644	8645	8646	8649
8399	8402	8403	8404	8407
8277	8280	8281	8283	8285
7911	7914	7915	7916	7919
Southwest				Southeast

Note that grid point 8403 is essentially at the Northwest Pacific deployment site.

These data consist of the following time histories, recorded at 1-hour intervals:

WD Wind Direction from which the wind blows, clockwise from true north, in degrees (meteorological convention)

WS Wind Speed; 1-hour average of the effective neutral wind at 10m height, in m/sec

ETOT Total Variance of Total Spectrum, in m^2

TP Peak Spectral Period of Total Spectrum, in sec.

VMD Vector Mean Direction of Total Spectrum to which waves are traveling, clockwise from true north, in degrees (oceanographic convention).

The following six variables are from dividing the directional wave spectrum into two components, a “sea” and a “swell”:

ETOT1 Total Variance of Primary Partition (sea), in m^2.

TP1 Peak Spectral Period of Primary Partition (sea), in sec.

VMD1 Vector Mean Direction of Primary Partition (sea), same rules as VMD.

ETOT2 Total Variance of Secondary Partition (swell), in m^2.

TP2 Peak Spectral Period of Secondary Partition (swell), in sec.

VMD2 Vector Mean Direction of Secondary Partition (swell), same rules as VMD.

M01 First Moment of Total Spectrum

M02 Second Moment of Total Spectrum

HS Significant Wave Height, in m.

DMDIR Dominant Direction following Haring and Heideman (1978) procedure

ANGSPR Angular Spreading Function following Gumbel, Greenwood and Durand (1953) procedure.

INLINE In-line Variance Ratio called Directional Spreading by Haring and Heideman (1978)

Typhoon Hindcast Local Wind-Driven Current Data:

Hindcast local wind-driven current for 25 intense typhoons at the Northwest Pacific site are from BNI.

These data reside on a floppy disk, created by BNI. This floppy disk has 1 zipped file called *local.wind.currents.zip*. This file contains 1 file for each of the 25 grid point around the site, named *local.gridno*, where *gridno* is the Oceanweather grid point number. These files can be extracted with commonly available programs such as WinZip. Each extracted file is 173 Kbytes in size, so that 25 sites would need about 4 Mb of disk space to hold, which is not very much.

These data consist of the following time histories, recorded at 1-hour intervals:

CD	Current Direction to which the current flows, clockwise from true north, in degrees (oceanographic convention)
CS	Current Speed in m/sec.

Typhoon Track Data

If general data is being studied at the Northwest Pacific site, an option exists to remove times during which typhoons are affecting the data, since it is known that this set of data is not accurate for typhoons. In order for the program to achieve this the typhoon tracks and parameters that define the typhoon intensity are needed. These files were obtained from a CD-ROM provided to the project as a joint release from the Navy Meteorology and Oceanography Command, Fleet Numerical Meteorology and Oceanography Detachment, and the National Oceanic and Atmospheric Administration, National Climatic Data Center. The CD-ROM is known as the Global Tropical/Extra-tropical Cyclone Climatic Atlas (GTECCA). The files for the 174 typhoons that passed within 600 km of the site (as described in Section 6.6.5.3) are saved by name on two zipped files called *74-95tracks.zip* and *48-92tracks.zip*. The first has the information on the 25 typhoons that were hindcast by Oceanweather, the second has the remainder of the 174 typhoons. The program estimates the wave height at the deployment site for each time, and if it is greater than a user-prescribed value the hindcast global data is excluded as it is read by the program. At the moment, the procedure is simply used to exclude data during the typhoons, that is known to be not very accurate, but a logical step would be to replace data in these missing time periods with data estimated from the typhoon parameters, using for instance the Cooper parameters (see Section 6.7.2) preferably after re-tuning these parameters to typhoons in this region. In this way, a reasonable estimate of the wind, wave and current data would be available over the full range of values from calm seas through super-typhoons.

6.6.4 Output of Results

All tables and plots are first displayed on the screen.

Tables and other numerical data are then saved on a file called *mobenv.out*, stored in ASCII format.

Plots are stored in individual files using encapsulated postscript (*.eps) format. The names of these files are derived from the sequence of decisions that result in the plot, followed by the word *plot*. For example: the file names: *HS.histogram.plot* or *ETOT.fit.lognormal.plot*

For both plots and tables, the criteria used for selecting the variable time series are shown with the output, as well as the actual variable being analyzed.

Plots created by MOBENV can be customized by the user if desired. The program should be exited, and then the figure can be changed by command line requests. For instance the command ylabel('new label') replaces the label on the vertical axis of a plot with the words *new label*.

6.6.5 MOBENV Sessions

A *session* with the program MOBENV is defined as a period of time that the program MOBENV is being used, during which a particular set of fixed criteria for the selection of data are in effect. For instance if the user is studying typhoon conditions for typhoon Kit at the Northwest Pacific site, this (along with other more detailed criteria enumerated below) constitutes a session. The lowest level defines the criteria that will be used to read the source data, and the highest level does statistical processing. A new session progresses from Level 1 to Level 4, but the user can move up and down from Level 2 to Level 4. No return to Level 1 is offered, since that involves changing the criteria used to choose the data, and a new session would be required. The levels are defined in the following subsections.

A MOBENV session is conceptually divided into four levels. The session flowchart for operations looks like the following:

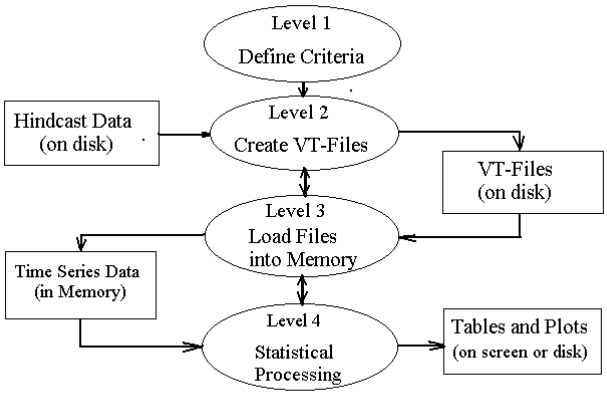

Level 1 defines the criteria used to collect the source data from archived hindcasts.

Level 2 reads these source data onto disk files called vt-files (variable's time-histories). They stay there until removed by the user, or overwritten in a subsequent session. Since the capacity of a computer disk is quite large, a large number of variables can be collected and written into vt-files ready for processing by MOBENV. All of these files, during a session, are subject to the same criteria.

Level 3 copies these vt-files into memory. Due to the more limited memory of a computer than disk space, the analyst should keep in memory only the files that he is using at any time and drop the rest.

Level 4 then takes the data that is now in memory (which are simply time histories of various variables chosen using the criteria of Level 1), and performs statistical analysis on them.

He may leave the program MOBENV, leave the MATLAB environment using the MATLAB *save* command to save the contents of the workspace, and then return at later time, and re-enter MATLAB and MOBENV where he/she left off. MOBENV will remember the criteria set before the break, and will continue the new session with the same criteria. When the user reenters the program after a previous session, he/she will have two choices. Continue as in the old session, preserving the memory of the selection criteria previously chosen, and entering the program at Level 2, or start a new session, wiping out the memory of the program of the previous session, and entering at Level 1.

Another advantage of this option is that, should the program crash due to performing some illegal operation, the user can re-enter without having to set up the criteria and load the needed vt-files.

6.6.5.1 Level 1 – Defining Basic Criteria for the Session

In a given session, since joint statistics may be asked for, data are read from the source files that are consistent from variable to variable. Thus, it would not make sense to try to create joint statistics at two different sites, or at the Northwest Pacific site from a year of general data and a set of five typhoons (that may not have even occurred in that year). Thus, the session criteria are set immediately and apply for the whole session.

The user starts a session at the lowest level (Level 1) of the program by typing the word *mobenv*. He then selects the desired criteria as follows:

Type of data:	Can be either General Data from global hindcasts or Typhoon Data from typhoon hindcasts.
If General Data:	Years to be included (sequential) Days of the years to be included (sequential) H_s used to exclude time periods for typhoons in the region (see Section 6.6.7.1) Location of site (grid point number)
If Typhoon Data:	List of typhoons to be included Random or fixed path selection: If random path, choose a grid of 2x2 or 3x3 or 4x4 points in 2^0 region (see below)

The Oceanweather global wind and wave hindcast and the BNI local wind-driven current hindcast extend from 1974 through 1996. The NRL global current hindcast extends from 1979 through 1996. Thus, if the user wishes to look at both data in a session, he should limit himself to the overlapping years 1979 through 1996.

6.6.5.2 Level 1 – Including only Data that Occurred While One Variable is Between Certain Bounds

Another criterion that can be adopted at this time, is to limit all data to be that which occurred while one variable known as the conditioning variable is between user-defined limits. Thus, for instance, the user may wish to examine only the data that occurred while the wind was blowing from between the N and E directions. By setting the wind direction as the conditioning variable, and choosing limits of 0° and 90° the program will perform the following. Whenever it reads wind, wave or current data, from a hindcast file, it will check to see whether the wind direction is between N and E and only if it is will it include that data. Obviously the narrower the bounds set by the user, the less data the program will find that conforms to this criterion.

6.6.5.3 Level 1 - Excluding Typhoon Data from General Data

The wind, wave and current data from the global hindcast at the Northwest Pacific site includes several days each year during which typhoons were in the region. During these

periods, the hindcasts are not likely to be as accurate as they are at other times, since typhoon events change more rapidly in time and space than the global hindcast model was designed for. So an option was included in MOBENV to remove data which contain significant effects from these typhoons at the deployment site.

The purpose of this was to enable the user to separate more clearly the data recorded when typhoons were not affecting the metocean conditions, from the data recorded when typhoons were nearby. In this way, the user has better control of the accuracy of the data he/she is using. The program estimates what periods of time have significant typhoon activity at the site and deletes these times from the time histories of metocean variables read into the vt-files.

Using a database of typhoon track information, and the Cooper parametric equations described in Section 6.7.2, the time history of significant wave heights at the site is estimated for the 174 typhoons that passed within 600 km of the site during the hindcast period, and, during these typhoons, whenever significant wave heights exceed a user-designated value, the data are not included in the data to be studied.

Although the same process could have been carried out for other sites where typhoons are present, (including Sea of Japan, Gulf of Arabia and several transit sites) this was not done, since these sites are presently not considered likely to be used for design, the conditions being milder than the Northwest Pacific, or the North Atlantic.

6.6.5.4 Level 1 - Random and Fixed Track Options for Typhoons

The following describes a procedure that was adopted to expand the wind and wave statistics generated from the 25 typhoons hindcast by Oceanweather.

The rational behind this process is that the randomness in the characteristics of the typhoons that pass by a given location can be thought of as being due to two separate properties of the typhoons:

1. variations in peak intensity at its center (loosely described by the category 1, 2 … 5) from storm to storm
2. randomness in the track of the storm

We could have selected the 22 typhoons that gave the highest wave height or wind strength in 50 years, at the deployment site. On the other hand, we selected the 22 most intense typhoons in 50 years that passed through a 2° block surrounding the deployment site. This latter selection is more efficient if we know the geographical distributions of the typhoon tracks, since we are then selecting the typhoons based only on intensity and can use our knowledge of the variation of the storm track to generate the path randomness, thereby effectively expanding the total set of typhoon intensity/path combinations. Simplistically, if we have selected the 22 most intense typhoons, regardless of how close they came to the site, we can consider them to move in, say, 20 different paths, and get the equivalent of 440 separate intensity/path combinations. It would take 440 actual typhoon

hindcasts to create the same amount of information if the typhoons had been selected based on the waves or wind at the site itself.

An analysis of the most intense typhoons in 50 years that passed through a 2° block surrounding the deployment site and those passing through a 4° block showed that there was no significant difference in the intensities of the storms that entered these two blocks. Therefore, we can say that the paths of intense typhoons are reasonably random within the 4° block, and that the 22 selected typhoons reasonably represent the 22 most intense in the 4° block also. Variations in typhoon tracks of 4° will however make significant differences to the wind and waves seen at a fixed site, so a procedure has been adopted that accepts these typhoons as the 25 most intense, regardless of local track details, but then provides some randomness in the track. This procedure is perhaps not the most rigorous possible, but, for the purposes for which MOBENV was designed, should provide a reasonable estimate of the effects of track variability.

If the user is looking at typhoon data at the Northwest Pacific site, he is asked to choose between two options, the fixed track option and the random track option. If he/she chooses to use the fixed track option, the wind and wave information is gathered at the deployment site.

However, if the user chooses the random track option, wind and wave data are collected from 2 x 2 = 4 grid points (or 3 x 3 = 9, or 4 x 4 = 16 sites, if the user chooses one of these). These sites are in a 2° square grid surrounding the deployment site. All these data are used in generating statistics, and if return period computations are requested, data from each such site are weighted by ¼ (or $^1/_9$ or $^1/_{16}$, respectively). The assumption implicit in this is that allowing the observer to be randomly positioned around the 2° block is equivalent to allowing the typhoon the same randomness in its track.

The effect of this is that there are effectively nxn typhoon histories created. Thus if the user selects 4 x 4 = 16 random tracks, for each typhoon there are effectively 16 typhoons with the same intensity as the original one, but with 16 different tracks, each displaced a little from the true track, this displacement being the vector distance of the grid point from the deployment site. All the statistical processing simply treats these as 16 typhoons, except for the computation of return period (Section 6.6.7.6). This computation should be done with all 22 of the most intense typhoons in the 2° box in the last 50 years. Since these were (thankfully) not 16 x 22 real typhoons of this intensity in this region in the last 50 years, the return period computations are performed treating each typhoon as a typhoon with 1/16 weight.

6.6.5.5 Level 2 – Collecting Data from the Source Files

After the session criteria are set, the user moves to Level 2 where he/she then selects any number of individual variables (e.g., H_s) to extract from the source files (according to the session criteria) and save on disk as "vt-files". These variables can be read from any of the appropriate sources, as follows.

If General Data: Oceanweather global hindcast.
NRL current hindcast
Local wind-driven currents

If Typhoon Data: Oceanweather typhoon hindcasts.
Local wind-driven currents
(NRL current hindcasts not available, since they are only for 18 years, whereas the typhoons are spread over 50 years.)

These vt-files are not erased from the disk by the program, allowing the user to reenter the session at a later time without having to set criteria and create vt-files. The user can erase these files at his leisure after finishing the session. If they are not erased, they will be over-written, as required, by subsequent sessions.

At Level 2, the user has the following formal options:

- See what vt-files already exist (on disk)
- Create another vt-file (on disk)
- Stop execution of the program
- Move to Level 3 to process existing vt-files

For processing the time series data, the user will then move to Level 3, as described below starting at Section 6.6.5.5

6.6.5.6 Level 3 – Reading Data into Memory

In Level 3, the user can read any of the vt-files from disk into memory. Only after these data are in memory, can they be analyzed, in Level 4, to produce single variable or joint-statistics. So, the next step is to read data from vt-files into memory.

If the user wants to add variables into memory that were not read into vt-files, he/she must drop back into Level 2 and create new vt-files from any environmental variables, and then come back to Level 3.

Note that the user cannot go back to Level 1 and change the criteria that define the session, but must start a new session to achieve this.

6.6.5.7 Level 3 - Creating Time Series of Functions of Variables

By the time the user is leaving Level 3, he/she has loaded the time series data for one or more variables into memory, from the corresponding vt-files.

Before actually doing any statistical analysis in Level 4 he/she has one more option. Create a new time series from one or more time series that are already in memory using any function of the existing series he/she chooses to program. Thus, if the user has read variables x_1 and x_2 into memory he/she can create a third variable $x_3 = f(x_1,x_2)$. In general there is no formal restriction on number of variables created or used in the function, and

we can create m variables from n existing variables (or even from variables created with this option in a previous command), using any functions f. However, each new variable must be created in a separate call to this option, since the updating of the variable count is done by the program, out of the control of the user. Thus for i = 1…m, we can generate $x_i = f_i(x_1,x_2,x_3…x_n)$, where x_1,x_2 … are any of the variables created up to that time, provided again that each x_i is created in a separate call to this option.

This is a rather powerful option since it allows statistical process of functions of the originally hindcast variables.

For instance, if it was decided to keep the MOB aligned with the wind, it could be used to find the component of the current perpendicular to the MOB axis. This would be achieved by defining a new variable that is the component of the current in the direction perpendicular to the wind. This can be easily computed from the wind direction, current direction and current speed.

As another example, if drag coefficients in the longitudinal and transverse directions were assigned to the MOB in air and water, the total drag force from wind and current could be computed in these directions. For this the new variable in the longitudinal direction would be the drag force computed from the wind speed and direction and the wave speed and direction and the direction of the MOB axis (either held fixed or defined from the wind or wave directions).

As a final example, using a numerical hydrodynamic model of the MOB such as WAMIT, a user could run a series of unit waves of varying peak period and direction, and estimate some peak response during a 6-hour period, for each such wave. Then, fitting a surface to this response as a function of wave height (linearly), period, and direction, the response of the MOB could be simulated over 20 years, say, and the extreme response for, say, 100 years could be estimated.

When requested in Level 3, the program turns control over to the user to add lines of code that create the new variable in memory. The following explains how this is done, using a simple example. In this example, it is assumed that there exist two variables x_1 and x_2 that have been read into memory, and these are the direction θ and speed v of the global current. These have been stored in locations 2 and 3 in memory, respectively. It is desired to compute the current component towards the East from these variables using the relationship:

$$v_x = - v \sin(2\pi\theta/180) \qquad (6.6\text{-}1)$$

After requesting the option to develop a new variable, the user presses the return key twice to get the prompt k>>.

The user will then type two lines, each followed by pressing the return key.

The first line defines the new variable (that will be loaded into memory in the next available column, *ndb*, in the variable storage matrix *data*.

data(:,ndb) = data(:,2)* sin(2*pi*data(:,3)/180);

The variable *data* is the name of the array stored in the program, and must be used. So data(:,2) and data(:,2) are the strings of data associated with the second and third variables in memory, namely θ and v, as assumed above. *ndb* is the count assigned by the program to the variable that is about to be created. Thus data(:,ndb) must be the left hand side of the last line of code that creates the new variable, data(:,n) must be used to refer to the nth variable in memory. The semicolon at the end stops the program from displaying the full time history of the new variable on the screen and, without it, the guidelines for creating the new variable are not displayed on the screen.

After defining the functional relationship between the existing variable(s) and new variable, a second line is then required to provide a name for this new variable. This name is stored in the variable *dbname* and looks something like this:

dbname(ndb,:) = ‘x-current ‘;

The name, (between the apostrophes), *x-current* , in this example, must be exactly 13 characters long. (Note that in the guidelines on the screen it uses asterisks, * *, instead of apostrophes, ‘ ‘, since the use of apostrophes would terminate the display to the screen.)

Press return at the end of the command.

If the user makes a mistake, he/she can simply retype it (unless the error terminates the program). To assist the correction, the user can use the up arrow to repeat the line he/she just typed.

After typing the above two lines, the user types the seven letters *return* to return control to the program.

If the user wants more details on this option, he/she should type *help keyboard* from the MATLAB prompt, or read the section *called Stepping Through Code and Using Keyboard Mode* in Section 3 of the MATLAB manual *Using MATLAB*.

6.6.6 Time Intervals for Data

For the general data option, the program can read, for any chosen site:

- the Oceanweather global wind/wave hindcast data at 6-hour intervals
- the currents from the NRL hindcasts at 3-day time intervals
- the local wind-driven currents computed by BNI at 1-hour intervals

In order to be able to compute joint statistics, or plot concurrent time histories, the time intervals from these three sources must match. 6-hour steps have been chosen for this option. If the 3-day currents had been interpolated to 6 hours, the user might forget the

original time scale, and, moreover, the interpolation would not add any real accuracy to the statistics. To create a vt-file, the data value at any NRL hindcast time (recorded at 3-day intervals) is simply repeated 6 times for the 6-hour intervals nearest it. On the other hand, the appropriate value every six hours is selected for the local wind-driven currents (recorded at 1-hour intervals).

6.6.7 Level 4 - Analysis Options for Single Variables

The following describe the options that are available in Level 4 to study and analyze the data that have been read into memory in Level 3.

6.6.7.1 Time Histories

The simplest processing is simply to print and plot the time series of any variable, or of more than one variable on the same plot. If more than one variable is to be shown on one plot, to avoid poor representation of two variables that are greatly different in magnitude, both can be scaled, if requested, by dividing by the maximum value, before they are plotted. The user can supply the range of the times to be included in the history, defaulting to all times selected in the Level 1 criteria.

Since the user had the option of selecting non-continuous blocks of data in Level 1 (e.g., one or more typhoons, or certain days in certain years) the data plots may show discontinuities from one time region to another. No attempt has been made to show the complicated times on the time axis, these times being determined from the start of the data saved on the vt-files.

6.6.7.2 Simple Statistical Quantities

The simplest level of processing available for any variable is to compute the maximum, minimum, mean and standard deviation of the variable. These are computed for all variables in memory and are displayed on the screen and saved on the output file.

6.6.7.3 Probability Distribution (Histogram)

The user can request that the program compute and plot a (probability) histogram for one variable. The user can supply the range of values to be included, (defaulting to all data) and the number of equally spaced “bins” to be used.

The program runs through all data and, if it is within the range of values specified for a bin, it is counted in that bin. The final distribution is found by adding the number of entries in each bin and dividing by the total number of values included in the set.

The final result is a table that gives for each bin the range of values to be included in that bin, and the probability of the variable being in that range. This table is also displayed as a plot showing the probability for each bin.

6.6.7.4 Cumulative Distribution

The cumulative distribution can be determined for any variable, including only the range of values chosen by the user (defaulting to all). The program determines the proportion of the data that exceeds various values of the variable. This is saved as a table and as a plot.

6.6.7.5 Fitting Cumulative Distribution Functions (CDFs) to Statistics

The main value in determining the cumulative distribution is to enable the actual data to be extrapolated to higher values for design purposes. To do this, the cumulative distribution is found as in Section 6.5.3.4 and then an analytical function is determined with parameters that allow the function to be fitted to the distribution. The function available has one or more of these parameters, and can be any one of the following distributions: (McClelland and Reifel (1986))

Normal
Lognormal
Gumbel (Extremal type I)
Fretchet (Extremal type II)
Weibull (Extremal type III)

For any of these, the distribution function from the data is printed and plotted along with the distribution function.

The following define these functions, using either the cumulative distribution function F(x) or the density function

$f(x) = \partial/\partial x(F(x)) = F'(x)$.

Normal

This is a function of two parameters, μ and σ.

Lognormal

The lognormal function has two parameters, μ and σ.

Gumbel (Extremal Type I)

This function is defined by the two parameters, ε and θ.

Fretchet (Extremal Type II)

This is defined by the two parameters, α and θ.

Weibull (Extremal Type III)

This is defined by parameters a and b.

6.6.7.6 Return Period Calculations

A valuable calculation for variables whose values increase with the intensity of loading (such as significant wave height, or current speed) is to estimate the return period associated with the variable. The return period R is the mean waiting time for a given event, or equivalently one can say that this event will occur, on average once in R years. The return period is a function of the value of the variable, increasing with the variable. This relationship can be computed by MOBENV for either general data or typhoon data, but the computation is different in each case, as described below:

It should be noted that the user should include all available data for a variable when performing these calculations, since the return periods are quite sensitive to the extreme values of the variables and it is important to get as accurate a distribution of these values as possible, which is achieved by including all available data. For general data, this means including all days for all years, while for typhoon data it means including all typhoons.

The final table and plot shows the value of the variable against the return period.

General Data

For general data, not typhoons, the data used are the full time series for as many years as are available. The cumulative distribution is found for the data, and one of the above cumulative distribution functions (CDFs) is then fitted to it. Then at all values of the variable, from the distribution function, the return periods are determined, as follows:

At any value of the variable, x, the CDF gives the probability, p, of being less than x. The probability of exceeding x is $q = 1 - p$. Since the data are recorded at 4 times per day, there are $365.25 \times 4 = 1461$ records per year. So, in one year, on average 1461q will exceed x. Thus, the return period associated with x is $1/1461q$.

It should be kept in mind that although it is mechanically possible to estimate return periods in this way at sites where typhoons occur, they will not be very accurate, since the accuracy of the global hindcasts is not high during typhoons. (See section 6.2.1, for instance). At the Northwest Pacific site, the typhoon data should be used as described below.

Typhoon Data

For the Northwest Pacific site, for the reasons just given, return periods should not be computed from the general data and the typhoon data should be used instead. However, these data do not represent the full population of values, and consist only of values near the extreme values. But, although the typhoon data can reasonably be expected to include the highest values during the 50 years from which the typhoons were chosen, the distributions of the metocean variables will not represent the true long-term distributions well. The reason for this is that these distributions should be determined by including a number of other typhoons that were not hindcast. Therefore, the return periods from the

typhoon data use only the maximum values of the variables in each typhoon, and are computed as follows:

First the data for each typhoon are scanned to get the maximum value that occurred for each typhoon. Then the cumulative distribution is found for these and a cumulative distribution function (CDF) is fitted to these data.

At any value of the variable, x, the CDF gives the probability, p, given a typhoon, that the maximum is less than x. For the same conditions, the probability of exceeding x is $q = 1 - p$. Since we have 22 hindcast typhoons in 50 years, each typhoon represents an occurrence rate of $22/50 = 0.44$ times per year. So, in one year, on average, $0.44q$ will exceed x. Thus, the return period associated with x is $1/(0.5q) = 2/q$.

An argument can be made for modifying the CDF as follows, and this has been adopted in the code. If there were more typhoons over a period longer than 50 years we would have a smaller distance between the maxima of the various typhoons, and so it is more accurate to treat the maximum from each storm as representing the midpoint of a continuous range. Thus, the maxima for each typhoon can be ranked from the smallest to the largest as shown in the following table, and the resulting probability of exceedance is as shown. Row 3 shows the CDF for the discrete assumption (not used) and row 5 shows it for the continuous assumption (adopted).

Rank of Storm	1	2	3	…	20	21	22
Number Greater than this: Discrete Assumption	21	20	19		2	1	0
Probability of Exceedance: Discrete Assumption	21/22 = 0.955	20/22 = 0.909	19/22 = 0.864	…	2/22 = 0.091	1/22 = 0.045	0.00
Number Greater than this: Continuous Assumption	21.5	20.5	19.5		2.5	1.5	0.5
Probability of Exceedance: Continuous Assumption	21.5/22 = 0.977	20.5/22 = 0.932	19.5/22 = 0.886	…	2.5/22 = 0.114	1.5/22 = 0.068	0.5/22 = 0.023

Table 6.6.7.6-1 Storm Ranking Example

6.6.8 Analysis Options for More Than One Variable

6.6.8.1 Scatter Diagram

A scatter diagram is a simple but powerful way to evaluate the correlation between two variables. It is plotted on a graph with each axis representing one variable. For each time point, the values of the two variables are read and plotted as one point on the graph. The result is a lot of dots, one per time point, from which trends may be spotted. If the data lie closely along a curve, there is a very high correlation between the two variables. If the data are almost uniformly spread there is very little correlation and the two variables are essentially independent. Such a plot may show varying correlation over different parts of

the space, a characteristic that would not be noticed in mathematical summaries of correlation such as correlation coefficients described in Section 6.6.8.2.

The user can choose the range of variables to be included in the scatter diagram, defaulting to all the data.

This option provides a plot, but there is no numerical data is provided with this option. However, quantitative data is available with the correlation coefficient option described in Section 6.6.8.2.

6.6.8.2 Correlation Coefficients

The correlation coefficient is a measure of the closeness of fit to a straight line. The correlation coefficient is defined as

$$\rho = R^{1/2} \tag{6.6-1}$$

Where:
$$R = \Sigma(y_i' - Y_m)^2 / \Sigma(y_i - Y_m)^2 \tag{6.6-2}$$

y_i are individual values of y

Y_m is the mean of the individual values of y

and y_I' are the values of y estimated from the straight line of best fit

In Figure 6.6.8.2-1, the values of ρ are shown for various situations.

The correlation coefficient matrix is a matrix of correlation coefficients for all variables. It is computed for all variables in memory, when requested, and shown in a table.

6.6.8.3 Joint Distributions (Histograms)

The user can request that the program compute and plot a joint probability histogram for any two variables. The user can supply the range of values to be included (defaulting to all data) and the number of equally spaced "bins" to be used, for each variable separately.

The program runs through all the data and, if, for a given time, both variables are within the ranges of values specified for a bin, it is counted in that bin. The final distribution is found by adding the number of entries in each bin and dividing by the total number of values included in the set.

The final result is a matrix that gives for each range of values of each variable, the probability of the variable being in that bin. The data are also plotted as a three-dimensional plot showing the probability of being in each bin.

6.7 Wind, Wave and Current Events and their Dependence on Global Typhoon Descriptors

6.7.1 Introduction

The principal storms in the Western Pacific are the typhoons that sweep through the region several times a year. These are characterized by their high winds rotating counterclockwise about a center which moves over the ocean. A study was performed that examined the wind, wave and current data seeking simple patterns that can be associated with the characteristics of the typhoons.

The first part of the study used a simple wind and wave model suggested by Cooper (1988), from a study in the Gulf of Mexico. In that earlier study, the wind, waves and currents were first found for a number of typhoons using numerical (hindcast) models. The wind and wave model was similar to the model used by Oceanweather to predict typhoon winds and waves for this current project. Then, the typhoons were assumed to be able to be described by a set of parameters, and the relationship between these typhoon parameters and a set of wind, wave and current parameters in the region of the typhoons was sought. In the present study, an examination of the accuracy of using those simple models was made.

The second part of the study was to examine the evolution of the wind, waves and currents as the typhoons pass by, and in particular to attempt to relate the characteristics of these items to the parameters that are used to describe the typhoons. The archived hindcast wind, wave and current data was plotted on a plan view of the ocean covering up to 1000-km square. These plots showed the wave significant heights and directions, wind speeds and directions and current speeds and directions, using contour plots and arrows at a large number of grid points. Plots were made during the evolution of four typhoons and at the peak of all the 25 typhoons that were hindcast. From these, observations were made about the relationship between wind, wave and current and the typhoon parameters.

6.7.2 Comparison of Simple Wind and Wave Models with Hindcast Model

The typhoons were characterized by 3 parameters:

δP, the pressure deficit at the center of the typhoon (mb)

V_f, the forward speed of the typhoon (m/sec)

R_m, the radius to maximum wind speed (m)

The wind and wave variables studied were:

W, the one-minute wind speed at 20 m height (m/sec)

α, the wind deflection angle relative to the tangent to the circle drawn around the storm center at the point being considered, positive angle being toward the storm center. This is indicated in Figure 6.7.2-1.

H_s, the significant wave height (m)

T_p, the spectral peak wave period (sec)

φ, the average wave deflection angle (defined as for α)

These wind and wave variables were considered dependent on the above three typhoon parameters, as well as the location of the point considered:

r, the radius from the center of the storm

θ, the angle relative to the line drawn at right angles to the storm direction of motion, on the right side looking along the storm track. This is indicated in Figure 6.7.2-1.

Equations including a number of constants were selected by Cooper to relate the wind and wave variables to the typhoon parameters. These constants were determined by a least squares fit from the data from the numerical wind, wave and current models.

The first part of the present study examined whether the parametric equations and constants determined by Cooper for typhoons in the Gulf of Mexico are also valid for the typhoons hindcast in the Western Pacific. Four of the 25 typhoons run by Oceanweather were selected for the study (they are described in Section 6.7.2.1). The wind and wave parameters W, β, H_s, T_p, φ were computed at a grid of points surrounding the eye, from the typhoon parameters δp, V_f , R_m, and these were compared with those derived by Oceanweather from the numerical models.

6.7.2.1 Selection of Typhoons

Oceanweather provided typhoon hindcast results for a grid of about 2000 points covering an area about 1000-km square, located centrally around the site, a portion of the area about 3000-km square that was used in modeling the typhoons. Four typhoons were selected from the 25 hindcast by Oceanweather. The criterion for selecting these was that the storms should have passed close to the Northwest Pacific deployment site near their most intense period. In this way, a large area of ocean surrounds the storm, where these comparisons were made.

The two parameters δp and V_f were found from data on the Global Tropical/Extratropical Cyclone Climatic Atlas (GTECCA), a CD-ROM produced jointly by the Fleet Numerical Meteorology and Oceanography Detachment, National Climatic Data Center. This CD-ROM lists, for all the significant typhoons in this century, the histories of the typhoon characteristics, including the above, the pressure at the eye of the typhoon, and the forward speed. The pressure deficit was found using ambient pressure of 1013 mb. The radius adopted was chosen after comparing the Oceanweather wind field near the eye at the time selected, and the radius provided by Oceanweather at the time when the waves at the site were largest, in their typhoon report, in the summary of the typhoons (Table 3, Appendix B).

Table 6.7.2.1-1 summarizes the four typhoons selected.

Year	Name	Date Selected at Peak of Storm (month,day,hour)	Central Pressure Deficit ΔP (mb)	Radius to Maximum Winds R_m (km)	Forward Speed V_f (m/sec)
1966	Alice	9/1/12	58	18.5	5.2
1976	Ruby	7/2/0	73	24.0	7.5
1987	Kelly	10/15/12	58	68.0	4.6
1990	Flo	9/17/6	123	31.0	4.2

Table 6.7.2.1-1 Properties of Selected Typhoons

Wind Speed:

Case (1) $r > R_m$

$$W = W_m \left(r/R_m\right)^a \quad (6.7\text{-}1)$$

where: $$W_m = 0.885 \left(5.6 \sqrt{\Delta P} - 0.5 R_m f_c\right) + V_f \cos\theta \quad (6.7\text{-}2)$$

and $$a = -0.38 + 0.08 \cos \theta$$

where: f_c, coriolis parameter = $2 \omega \sin$ (latitude)

and ω, the angular velocity of the earth's rotation = 7.29×10^{-5}

Case (2) $r < R_m$

$$W = W_m \{1-\exp(-3.1\, r/R_m)\} \quad (6.7\text{-}3)$$

Wind Deflection Angle:

$$\alpha = 22.0 + 10.0 \cos \theta \quad \text{(degrees)} \quad (6.7\text{-}4)$$

Note that this is wind direction to the direction of motion, in contrast to meteorological convention. For consistency, the hindcast wind direction was changed to this convention.

Wave Height:

$$H_s = 0.25\, W \quad (6.7\text{-}5)$$

Wave Peak Period:

$$T_p = a\, W^b \quad (6.7\text{-}6)$$

where: $a = 8.0 - 3.5 \cos\theta + 2.7 \sin\theta$ (different a from that used for wind) (6.7-7)

and $b = 0.143 + 0.138 \cos\theta - 0.074 \sin\theta$ (6.7-8)

Average Wave Deflection Angle:

$$\varphi_d = \alpha + a\,(^r/_{Rm})^b - 180 \quad \text{(degrees)} \quad (6.7\text{-}9)$$

where: $a = 144 + 39 \cos\theta - 25 \sin\theta - 15 \cos 2\theta$ (6.7-10)

and $b = -0.08$

Wind at 20m from Wind at 10m

W, the wind speed at 20 m was converted to the wind speed at 10-m elevation, using the logarithmic formula given in Section 6.3.1.1, before comparing with the hindcast values.

$$W(10) = W(20)\, \ln(10/z_o)/\ln(20/z_0) \quad (6.7\text{-}11)$$

z_o is the roughness length was computed (in meters) from

$$z_o = 10 \exp\{-17.7\, [W(10)]^{-0.23}\} \quad (6.7\text{-}12)$$

For winds over 20 m/sec, used the value of z_0 at 20 m/sec, namely $z_0 = 1.38 \times 10^{-3}$ m was used

6.7.2.2 Comparison of Wind and Wave Variables

The accuracy of the Cooper parametric equations is demonstrated by plots comparing each of the wind and wave parameters from the Oceanweather results with those from the parametric equations, in scatter diagrams, as shown in Figures 6.7.2-2 through 6.7.2-21. These plots are created by plotting a point for each location used. For each such location, the value of the variable (e.g., significant wave height) found by the Cooper equation is used as the abscissa and the value found by the Oceanweather hindcast is found as the ordinate. Points lying in a thin band at 45° indicate good fit, while a broad "line" or a curve other than a 45° line indicate poorer fit of these equations. These plots were created for each of the variables: wind speed, wind deflection angle, significant wave height, peak wave period, and wave deflection angle, and are shown in Figures 6.7.2-2 through 6.7.2-21. For comparison, the plots given by Cooper are shown in Figures 6.7.2.2-1 through 6.7.2.2-5.

Cooper's comparison was made over the full region of the hindcast, or about 400-km square. The present hindcast area was about 3000-km square, and, in order to make comparisons over the more intense part of the storms, evaluations were made over the

archived region, about 1000-km square. To speed up computations, only every 5th archived grid point was used.

Figures 6.7.2-2 through 6.7.2-5 show the wind speed comparisons. In general, the wind speeds predicted by the simple equations overpredict the lower winds rather badly, but are rather better for the (more important) higher wind speeds, near to the eye. This pattern follows that reported by Cooper in his Figure 2, reproduced here as Figure 6.7.2.2-1, although the scatter is somewhat larger in the current study.

The wind deflection angles are shown in Figures 6.7.2-6 through 6.7.2-9. The agreement of the two models is poor. This appears to be caused by the following effect. The wind directions from the Cooper model are based on essentially zero winds away from the center of the storm. In the typhoon hindcasts the typhoon winds were created on top of the existing ambient winds in the region. This has the effect of modifying the wind directions over a large part of the region being examined.

Figure 6.7.2.2-6 shows the wind field directions (not magnitudes) for typhoon 66ALICE, over a region covering the southern part of the typhoon, about 1000 km, by 650 km. It can be seen that the wind directions in regions more than about 400 km away from the storm center are almost unaffected by the presence of the typhoon. The predictions of the simple typhoon model will continue to show a circular (spiral) structure to the ends of the region being studied.

Wave heights are shown in Figures 6.7.2-10 through 6.7.2-13. The simple model overpredicts the lower waves, and underpredicts the higher ones near the storm center.

The peak wave periods shown in Figures 6.7.2-14 through 6.7.2-17 are perhaps more accurate for this study than those in Cooper's work, and although there is considerable scatter, the trend appears to be correct.

Figures 6.7.2-18 through 6.7.2-21 show the wave deflection angles. The scatter appears to be greater than found by Cooper, and the Cooper equations seem to overpredict this angle rather substantially.

6.7.2.3 Conclusion on Wind and Wave Variables Comparison

In summary, the simple equations appear to give reasonable estimates of wind speed and wave heights and periods, but not accurate enough for even early design use. Perhaps the coefficients could be tuned with the 25 hindcast typhoons, to represent reasonable predictions of typhoon wind and waves. Directions are not predicted well, but, if only the more intense part of the typhoon were considered, the agreement would presumably be better. This has not been pursued at this time.

6.7.3 Typhoon Wind, Wave and Current Study

For each of the 25 typhoons hindcast by Oceanweather, wind and wave data were provided at about 2000 grid points covering a rectangle about 1000 km square. These

points were on grid lines spaced at about 25 km. From these wind fields, BNI computed estimated currents using the program PWP {reference} from Dr. Jim Price of Woods Hole Oceanographic Institution, after modification by BNI. Currents were computed at 90 points on a 9 x 10 grid covering the same region.

A computer program was written to extract wind, wave or current data at any selected time during any typhoon, from a selected region of the archived area. For waves this program reads the significant wave height, HS and vector mean direction, VMD. For wind it reads the wind speed, WS, and direction, WD. For currents it reads the current speed, CS, and direction CD. It then plots the wind, wave or current field on a plan view of the region selected. On this view contours of HS, WS or CS are shown, as well as arrows showing the direction VMD, WD or CD (resp.), the length of the arrow representing HS, WS or CS. The lengths of the arrows are not consistent from plot to plot, but the scale is given by noting the maximum value recorded at the bottom of the figures and relating it to the longest arrow. The tail of each arrow is at the location where the data is read. Also shown on the plot is the "max. slope". This is the maximum difference in adjacent values of HS, WS or CS, divided by the corresponding spacing, in degrees, of the grid points used. This is therefore the maximum rate of change of the variable with respect to longitude or latitude, in units of m/degree, m/s/degree or m/s/degree.

The program reads all archived grid points in a selected region if the requested spacing is fine enough, or skips one or more grid lines of archived data if the requested spacing is coarser. Due to restriction on the program compiler, and the length of time taken to process the data, it was not possible to read the full set of 2000 grid points. To cover the full archived region, a coarser spacing was used, and at the original archived spacing a somewhat smaller region was required to be accessed.

The first task was to give an overview of the characteristics of major typhoons in the Northwest Pacific.

Selected for study was the typhoon Ruby in 1976, an intense typhoon which generated significant wave height of 11.1 m at the deployment site and accompanying winds of 43.6 m/sec. Note that the spacing of the grid shown is about 3 times the archived spacing, so some fine detail is missing. The storm center is moving in a generally ENE direction. Note also that at this region one degree of latitude or longitude is quite close to 25 km.

Figures 6.7.3-1 through 6.7.3-5 show the wind fields for 5 times 12 hours apart, as the storm passed near the site. Note that the winds are considerably stronger on the right hand side (facing the direction of storm travel) of the center. The radius to maximum winds for this storm is only 13 km, so the decrease in wind speed in the eye is not seen in these plots. As the air is forced toward the low pressure area at the eye, it rotates clockwise (in the Northern hemisphere) resulting in counter-clockwise rotation of the wind field. The result is an inward spiral of the air.

Figures 6.7-6 through 6.7-10 are the corresponding wave fields. Not shown here, of course, is the large amount of directional spreading that exists due to the rapidly changing

wind directions. Superficially the wave field resembles the wind field but the spiral created by the wave directions is an outward one, not inward.

Figures 6.7.3-1 through 6.7.3-15 show the currents created by the winds. The current fields are quite complex due to the changing winds and the effects of the rotation due to Coriolis effects, which tend to cause oscillation of the currents as described in Section 5. The complexity of the current field is seen in Figure 6.7.3-15 after the typhoon has traversed the region plotted. The model used to compute the currents does not consider horizontal interaction of the current at one location with that at another, so for the rapidly changing wind fields modification to these patterns may be significant.

6.7.4 Rate of Change of Significant Wave Height, Wind Speed and Current Speed During Typhoons

Because of the length of the MOB, and the possibility of varying forces along the MOB causing significant forces in the connectors between the modules, or requiring significant dynamic positioning action to keep the independent modules together, it is of interest to study the variation of the variables HS, WS and CS along the length of the MOB. Note that during the passage of a major typhoon it is expected that the MOB will be separated into its modules, each of which is probably about 1000 m long, depending on the concept, so variation across about 1000 ft are of more interest than within the full length of the MOB. Most concepts are particularly susceptible to variations of the current with horizontal location, but this study included wind and wave as well.

Eight typhoons were selected for this study. These include the four selected in Section 6.7.2 augmented by four of the more recent typhoons. The typhoons used were 66Alice, 76ruby, 81Elsie, 82Ellis, 87Kelly, 88Nelson, 90Flo, and 92Janis. The principal purpose of this study was to find the most rapid variation of HS, WS and CS with horizontal distance and to see whether this is likely to be design issue.

The first study was on significant wave height. Plots similar to those shown in Figures 6.7.4-1 through 6.7.4-8 were made for each of the 8 typhoons at a number of times as the typhoon traversed the region where data had been archived. At each time the rate of change of HS with horizontal location (per degree actually) was found from the plot. The time when this rate of change was greatest was recorded and that plot was saved. Thus Figures 6.7.4-1 through 6.7.4-8 show the wave field for each typhoon at the time when the rate of change of HS with respect to distance is greatest. Only the region immediately around the storm center is shown, and these plots have the same grid spacing as the archived data so all archived grid points in the region shown are included.

The above study of wave heights was repeated for wind speeds, resulting in Figures 6.7.4-9 through 6.7.4-16, and for currents resulting in Figures 6.7.4-17 through 6.7.4-22.

To see whether these rates of change of WS, HS and CS are simply correlated with the typhoon parameters Δp and R_m, the pressure deficit and the radius to the maximum wind, the plots shown in Figures 6.7.4-23 through 6.7.4-25 were made. Two separate sets of points are superimposed on each, each point representing one typhoon. For the first set,

the vertical axis represents the radius to the maximum wind and the horizontal axis the rate of change or either WS, HS or CS. For the second set, the vertical axis represents the pressure deficit. In none of these plots is there a clear trend shown for either set of points, so it must be concluded that the rate of change of WS, HS and CS are not simply related to these simple parameters.

Table 6.7.4-1 shows the maximum value of WS, HS or CS and the maximum rate of change with respect to horizontal distance over all the typhoons studied. Also shown is the maximum change expected across the length of one module, assumed to be 1000 ft (300 m).

	Wind Speed (m/sec)	Significant Wave Height (m)	Current Speed (m/sec)
Maximum Rate of Change (per km)	1.88	0.18	0.015
Maximum Value	55	17.6	2.17
Change Across Module Length	0.6	0.05	0.005

Table 6.7.4-1 Maximum Rates of Change of Wind Speed, Significant Wave Height and Current Speed

The conclusion from this table is that these are insignificant changes across the length of a module compared with effects like ocean and atmospheric fronts, and internal waves.

6.8 Recommendations

The work performed in this delivery order reflected a first attempt to assess and quantify the environment under which the MOB is expected to operate for the purpose of executing a better defined and safer design. In some ways, the work was incrementally developmental, particularly in the beginning of the project, due to its lack of precedence, uniqueness and vastness of applicable issues.

The generated product presents a solid foundation for design and input to the overall MOB Classification Guide. Nonetheless, as it is inherent to this kind of work, new lessons have been learned by simply doing the work and additional advances in gathering of environmental data are continued to be made. Some of these are deemed important developments for the design of the MOB but they were not part of the scope of work agreed upon to date for this delivery order. They are offered here as points of awareness, recommendations for consideration by the Government, and for possible future studies. It is believed that such studies will further improve the present product and will update it to

reflect new additional findings. In all, they will at the end result in a yet better MOB design.

6.8.1 Nonlinear Wave Effects on MOB

Nonlinear effects are important to fixed offshore platforms because the dimensions of their members are quite small (3 ft – 5 ft diameters typically) and drag forces thus dominate the wave loads, resulting in peak forces near the wave crest, where nonlinearities are especially apparent in surface elevation and water particle velocities. Semi-submersibles used in offshore oil operations are less susceptible to nonlinear effects since the forces on them are dominated by inertial forces that occur near the wave zero-crossing, where surface elevations are small and nonlinear effects on water particle accelerations are less significant. Conventional wisdom is to essentially ignore nonlinearities in the waves for design of conventinal semi-submersibles.

The question of how important nonlinear wave effects are for the MOB is not yet known, but this determines what the Environmental Specification should say about such effects. If nonlinearities have little effect on the forces on, or motion of the MOB, there is not a great need to quantify these effects, and the Specification can quickly identify the extent of the need to include them. On the other hand, if it is determined that nonlinearities make substantial differences to the design of the MOB, then considerable care should be taken in specifying these effects in the Specification and also in the Classification Guide.

There are two somewhat independent nonlinear effects that will be considered here:

(1) Effect on increasing the crest heights and possibility causing waves to hit the deck. The recommended study would give information on the crest heights of incoming nonlinear waves, but, as presented here, would not study the characteristics of the nonlinear reflected waves which are added to the incoming waves.

(2) Effect on MOB global responses. It is recommended that this be studied in some detail.

Some very advanced programs can handle 2^{nd} order 3-D waves (e.g., WAMIT). Most are limited to 1^{st} order waves and compute wave forces up to the mean water level, ignoring the extra loads that develop from the wave above the mean water level, and ignore the change of shape associated with nonlinearities (high crests and shallow troughs).

It is suggested that the study be confined to 2-D (long crested waves) at this stage. Long-crested seas are seas that are essentially running in one direction and give a reasonable picture of waves in the North Atlantic.

The degree of nonlinearity of a long-crested seastate can be estimated fairly well by:

(1) looking at the largest individual waves and seeing where their (H, T) lie within standard criteria of linear versus nonlinear kinematics for regular waves (See eqn 6.3-12, for instance).

or,

(2) actually running linear and nonlinear irregular wave simulations for the (Hs,Tp) and seeing how the resulting water particle kinematics differ from each other. Such simulations are state-of-the-art, but do exist (e.g., Zhang, (1991)).

The effect of nonlinear waves on MOB *responses* would then be examined.

Second-order waves could be analyzed using cutting-edge software like WAMIT, or make more approximate estimates using Morison equation wave loads, since, for extreme seastates, Morison equation gives a reasonable estimate of the wave loads. The latter is proposed here. Morison wave loads are considered quite accurate when the ratio of member diameter to wavelength is less than about 0.2. For storm waves, with periods of about 13 sec, wavelengths are about 900 ft, and Morison equation should be adequate for members up to about 175-ft diameter, which is considerably more than the size of members in all present MOB concepts. Thus, Morison equation simulations should be quite effective in studying the effect of nonlinearities.

The study can examine all concepts (for full evaluation) or one (for representative evaluation). The one-concept study would serve strictly as a representation for studying the nonlinear wave effects and be used as a quantitative indication of their importance. Depending on the findings, all other concepts can then be explicitly studied. A computer model for the concept(s) to be studied would first be created. Potentially, models currently being used in the work of Delivery Order 23 (Design Tools and Methodologies, Benchmark Analysis) can serve as the foundation for this modeling. Probably single modules would be analyzed since the MOB would be disconnected during a big storm, but it might also be of interest to study the connected MOB with shorter period and lower height waves.

Because of the importance of dynamics in the response, there would be no point in running a dynamic analysis with regular waves, but it is of considerable interest to compare the applied wave loads from linear and nonlinear waves. The first part of the study would then concentrate on finding the total applied loads (moments and translational forces) associated with linear and nonlinear waves. Very large waves of various heights and periods would be run by the MOB models in different directions, and would be modeled first by linear waves using the linear assumption of computing forces up to the mean water line only. Then, stream function or Stokes waves would be used, of gradually increasing order, 2^{nd}, 3^{rd} etc, with wave forces calculated.

In the second part of the study irregular waves will have to be developed, and various structural responses such as member forces and global motions will be monitored. Nonlinear free surface elevations would be generated from a nonlinear wave program. Water particle kinematics could then be generated in one of two ways:

1) by superposition of linear waves, the wave components having been generated from the nonlinear free surface history. Water particle motions are computed using "stretching" of water particle kinematics in the manner that has been developed and used quite extensively in the offshore industry.

2) using the water particle kinematics generated by the nonlinear wave program.

The motions of the MOB would first be predicted using strictly linear wave kinematics, using free surface histories generated to match the wave spectrum. These would have big waves in them, but the crest and trough heights would be statistically similar. This would be done for a number of wave histories that match the wave spectrum, and the statistics of the MOB response would be assessed. This would also be done for a variety of directions and increasing significant wave heights from strictly linear to including waves close to breaking.

The above analysis would then be repeated with nonlinear waves generated from the nonlinear program, over the same range of directions and significant wave heights. Nonlinearities would generate larger crest heights than would be found in the previous runs.

In this way, the importance of wave nonlinearities would be studied, and the need to include these effects in detail in the Specification would be decided.

6.8.2 Additional Description of Wave Spectra for Deployment Sites

The wave spectra in this Environmental Specification are characterized by (Hs, Tp, θ) for a choice of 1, 2 or 3 wave trains. Although this is probably enough, additional data can be presently obtained from Oceanweather's continuing development in this area for the full directional spectrum with a matrix of n_f frequencies by n_d directions. This is presently available for global data (at the four deployment sites) and it may be possible that Oceanweather have archived for their own records more than we have obtained to date for the typhoon hindcasts.

6.8.3 Refinement of Wind Data

Section 6.4.1.1 discusses the accuracy of the global winds from the NCEP/NCAR climatology. These data, at 6-hour intervals, miss the considerable detail associated with periods less than the 6 hours at which they were archived. The 6-hourly data should be quite satisfactory for determining fuel requirements needed to keep the MOB on location, provided the criteria adopted for the dynamic positioning system (DP) allow the MOB to be blown backwards and forwards with the varying wind strengths, attempting only to keep it on location in a long term average sense. However, if the MOB is to be kept more closely on site within time periods of the order of hours or less, or if operations such as aircraft operations are to be closely examined over time scales of hours or less, more detailed wind data may be needed.

An approximate recommendation has been given in this Specification for converting the 6-hourly means to means with shorter averaging periods, like an hour or less. Although this is probably satisfactory for mean values, it says nothing about the time variations of the wind speed or directions about those means. The variations of the wind speeds due to turbulence has been described in Section 6.3.1.3, for time scales appropriate to turbulent

air flow, typically minutes. There exists thus a gap in the data needed to describe wind variations with time scales of large fractions of an hour up to a few hours.

It is, therefore, recommended that additional wind data be sought in the region around the two primary deployment sites (North Atlantic, and Northwestern Pacific) that provide information on wind speed and direction variations, over time scales from several minutes up to a few hours, for as long a segment of time as can be found. Such data can then be used to supplement the wind data provided.

6.8.4 Rarely-Occurring Waves for Reliability Analysis

Estimates of extreme waves at the one in 100 years (annual probability of occurrence of 10^{-2}) level have been traditionally made by extrapolations from hindcasts of waves in historical storms. The only assumption is that the statistics of future storms will resemble those of the past. Data on historical storms generally extends over enough years that the extrapolation to 100-year conditions is reasonable. Most offshore structures and many vessels have been based on 100-year waves, with an estimate of the corresponding peak wave period. Working stress or LRFD design procedures are used that include significant factors of safety. There is general consensus that estimates of 100-year waves are reasonably accurate.

The MOB is to be designed by risk (reliability) calculations in which the actual probability of failure will be estimated. Prudent design, particularly for a structure of such extreme importance, requires this probability of failure to be at the 10^{-4} to 10^{-5} level. All seastates contribute in computing the estimated failure probability and estimates of seastates that occur at these same low probability levels are required for these calculations. Extrapolation of historical hindcasts to such low probabilities often leads to large statistical errors.

The offshore industry is starting to rely quite heavily on reliability methods in designing and re-certifying offshore platforms, and is encountering the same problem.

We are aware that a joint industry project is being currently assembled by the offshore industry to try to improve the accuracy of determining the probability of occurrence of seastates with these low rates of occurrence.

The basic idea is that the wind field in a hurricane can be determined from a relatively few parameters (peak wind speed, radius to maximum wind, forward speed, track, etc). Very low probability seastates come from combinations of storm track and storm intensity that have much lower probability than probabilities of the individual parameters. For instance, if we know the (preferably joint) distributions of the radius, peak wind speed and forward speed from 100 storms, we have strong estimates of the distribution of these parameters individually. Then, when we combine these randomly, but according to their distributions, we are able to create a large number of storms that satisfy the distributions of the parameters that characterize the storm, and we get a large database with which to estimate the statistics of the seastates. Thus, knowledge of the basic parameters at moderate probabilities can be combined to give seastates at very low probabilities.

The referred joint industry project has been proposed by oil companies to study this problem first in the Gulf of Mexico, and then in other regions, including the Northwestern Pacific which is of prime interest to the MOB. Under the current early plan, the first phase will be using the Cooper parametric equations to estimate the waves associated with a given hurricane. In the second phase, full hindcasts would be used, rather than the simplified equations.

The study is being currently put together and the Government could be a participant, with BNI being the active link between the project and the Navy in light of the work performed in this Environmental Specification, and to appropriately incorporate the findings as may be related to the overall data. Indeed, since the first phase is being conducted in the Gulf of Mexico, using the Cooper equations, no great secondary expenses from full hindcasts should be involved, and BNI could even carry out a parallel study in the Northwestern Pacific for the Navy. To accomplish this, a first study would be required to calibrate the Cooper equations to the storms in the Northwestern Pacific, since the study just performed has indicated considerable weakness in the unmodified Cooper equations in this region.

6.8.5 Correlation of Hindcast Data with Hurricane Bonnie Measurements

Last August 24, hurricane Bonnie occurred. There is currently information available on this storm including actual waves in hurricane Bonnie as measured from a NASA airplane. The data are significant because they are the very first measurements ever of the overall wave field associated with a hurricane.

The plane flew many passes through the eye of the hurricane over a several-hour period. It had a scanning radar altimeter (SRA) on board that measures absolute (slant) distances from the plane to a small patch of ocean (say, 20-m square). Then, using the known angle to that patch and the estimated instantaneous height of the airplane, it uses simple trigonometry to figure the vertical height of that patch. Thus, the instantaneous sea surface is determined. The SRA scans something like 45 patches laterally in 0.1 sec or less, then waits a 1/2 second or so and repeats.

The assembly of these patches over the path flown by the airplane can then be displayed as a topographical map, with white being crests and black being troughs. There are maps available showing the individual strips. These maps were then superimposed to make the composite figure which is presently available on the world wide web. Ed Walsh of NASA, who was directly involved in these measurements, plans to fly into future hurricanes this season, so we may see even more of these unique measurements.

It is a great opportunity to study these very recent real data and assess any correlation with the available hindcast data provided in this Environmental Specification**.** To assess the accuracy of the wave hindcast data, a hindcast could be commissioned to simulate hurricane Bonnie, in exactly the same manner the Northwest Pacific Typhoons were hindcast. Data would be archived for a region of the ocean large enough to cover the

swaths created by the NASA airplane described above. The wave data from the SRA on the airplane would then be compared with that produced by the hindcast.

6.8.6 MOBENV Enhancements

The program MOBENV is a valuable tool in examining the huge amount of data archived for this Specification and developing statistical information on them. In developing this tool, emphasis was put on the computational aspects and the user interface is perhaps not as elegant as it could be. MATLAB, which was the application used for developing MOBENV supports a graphical user interface (GUI) that was not used in MOBENV. Thus the program could be made to be menu-driven, instead of requiring the user to interact with the program in a prescribed sequence. Such enhanced GUI would make it not only more user friendly but further broaden and increase its use.

6.8.7 Improved Global Data When Typhoons are in the Region

A useful improvement to the hindcast data would be to attempt to improve the global hindcast at the Northwest Pacific site during times where the local weather is dominated by typhoons. The global hindcast is not very accurate during these times, due to the spatial and temporal scales of typhoons being too small for the global model. It might be possible to adjust the global data during these typhoons, to make it more accurate, so that the statistics generated from the global model would be closer to reality during these periods of time. Note that extreme conditions should still not be estimated from data adjusted like this, since the typhoon hindcasts themselves are more accurate and should be used. Nevertheless, for purposes such as operational availability, the improvement could be quite useful.

Two possible approaches could be used. The first would be to use the hindcast data from the typhoons that occurred during the period of time covered by the global data. The global wind, wave and current data at the Northwest Pacific site could be compared with the typhoon hindcast data at the same times, and adjustments made to the global data for these periods and other times when typhoons are near.

The second approach would be to substitute the wind, wave and current data during typhoons with data estimated from a simple parametric model such as the Cooper model that was evaluated in Section 6.7. The full set of 25 typhoons would first be used to tune the various parameters in the Cooper model, to conditions in the Northwest Pacific. With that successfully accomplished, we would have a reasonable model for predicting environmental conditions for all typhoons that occurred in this region. The global data during typhoons could then be removed and replaced by those predicted by the parametric model.

The second method would, of course, require initial work to estimate values of the Cooper parameters that fit the data best, but would almost certainly be more accurate, since it uses a database of the full set of 25 typhoons to create the simplified model of

Pacific typhoons. Once this simplified model of these typhoons is available, this model would provide a rational method of estimating environmental data while typhoons are in the region. The first method would be using fewer typhoons for the comparisons, since there were far less than 25 that occurred during the period of time the global model was run. In addition, the adjustments would have to be somewhat arbitrary, and it might be rather difficult to determine a rational basis for adjusting the global data during typhoons, since there would be no simple model to act as a guide.